

ARTICLES

Screening mechanisms in sedimentation

Michael P. Brenner

Department of Mathematics, Massachusetts Institute of Technology, Cambridge, Massachusetts 02139

(Received 28 April 1998; accepted 30 December 1998)

This paper considers a mixture of sedimenting particles at low Reynolds numbers and volume fractions. Simple theoretical arguments have long suggested that for a random suspension of particles in an infinite system, the fluctuations in the velocity about the mean should diverge with system size. On the other hand, experiments have shown no such divergence. The primary goal of this paper is to examine the effect of side walls on the predicted divergence in fluctuations, through theory, scaling arguments, and numerical simulations. Side walls lead to important modifications of the standard arguments. A scaling argument (based on wall effects) is presented to rationalize recent experiments by Segré *et al.* [Phys. Rev. Lett. **79**, 2574 (1997)]. The paper also briefly discusses the role of inertia in screening fluctuations in infinite systems when the particle Reynolds number is very low, and also the coupling between the velocity fluctuations and the mean sedimenting velocity. A physical argument suggests that in some circumstances the fluctuations give a leading order correction to the mean sedimenting velocity as a function of volume fraction. © 1999 American Institute of Physics. [S1070-6631(99)02104-2]

I. INTRODUCTION

The sedimentation rate of a mixture of monodisperse solid spheres in a liquid is a classical problem in fluid mechanics.¹⁻⁴ For slowly sedimenting particles, long ranged hydrodynamic interactions lead to a correction to the Stokes settling velocity⁵ U_s of a single sphere. In the limit of low volume fractions ϕ , theories predict the sedimentation velocity as^{3,4}

$$U_{\text{sediment}} = U_s [1 - 6.55\phi + O(\phi^2)]. \quad (1)$$

The $O(\phi)$ correction is due to the presence of a fluid back-flow arising from the sedimenting particles.⁴ Another elegant physical argument for this $O(\phi)$ correction is given in Hinch,⁶ who considers it arising from $O(\phi)$ corrections in effective properties of the medium around a test particle in a homogeneous fluid. The main assumptions in theories leading to the prediction that the correction to U_s is $O(\phi)$ are: (i) the neglect of inertia, since the particle Reynolds number Re_p is small; (ii) consideration of only two body interactions between the spheres; (iii) the particle distribution is random in the limit of small ϕ ; and (iv) the system size is infinite in the direction transverse to the settling. Experimental fits of the average settling velocity as a function of volume fraction show a roughly linear dependence on ϕ in the limit of small ϕ , although with a prefactor which is systematically smaller than 6.55.^{7,1}

The consistency of this theory was called into question by Caffisch and Luke,⁸ who pointed out that the assumptions listed above imply that the velocity fluctuations of the fluid diverge with increasing system size. A physical scaling argument for the divergence in fluctuations was given by Hinch.⁹ Experiments and computer simulations have given

contradictory evidence regarding the existence of this divergence: On one hand, computer simulations by Ladd^{10,11} support the conclusion, finding an increase in the size of the velocity fluctuations with system size.

On the other, two different types of experiments have been performed, both finding an independence of the fluctuations on system size: Ham and Homay¹² and Nicolai *et al.*^{13,14} studied the diffusion of a colored test particle during sedimentation, and extracted the effective diffusion constant of the particle. Systematic studies¹⁴ demonstrate that the diffusivity does not vary with system size when the smallest dimension of the cell is varied by a factor of 4 at fixed ϕ . A second type of experiment was recently performed by Segré, Herbolzheimer, and Chaikin,¹⁵ who used particle image velocimetry to record the velocity field in the center of the experimental cell at a fixed time. They found that by increasing the largest dimension of their cell, the size of the velocity fluctuations saturated, with an explicit dependence of fluctuations on the solid volume fraction ϕ over three orders of magnitude in ϕ . Their principal results are that: (a) the velocity fluctuations saturate at a scale of order $U_s \phi^{1/3}$; (b) the correlation length is of order $30a \phi^{-1/3}$, where a is the particle radius; and (c) experiments with varying system size demonstrated that the velocity fluctuations saturate for systems larger than approximately ten times the correlation length. Each correlated region in the experiment contains of order 3000 particles, indicating that the phenomenon is a many particle effect, breaking assumption (ii).

A single theoretical argument has been put forth to explain the independence of the fluctuations on system size. Koch and Shaqfeh argued that screening of the velocity fluctuations results from correlations in the particle

distribution,¹⁶ violating assumption (iii). Their central idea is that the particle distribution arranges itself precisely to cancel out the divergence in the fluctuations. By explicit computation, they found a single particle distribution which has this property. The distribution is characterized by a net deficit of exactly one particle surrounding any test particle. The theory predicts that the velocity fluctuations scale like U_s (independent of volume fraction) and that the correlation length scales like $a\phi^{-1}$, in contrast to the experiments.

The primary goal of this paper is to examine the effect of side walls on arguments leading to the prediction of diverging velocity fluctuations with system size. Although it is well known that side walls greatly modify the velocity field of a single particle falling in a container¹⁷ (e.g., in a cylinder the velocity far from a particle decays exponentially on scales farther from the particle wall separation, instead of like r^{-1}), this effect appears to have been ignored in theoretical discussions of sedimentation, which typically assume⁴ the system size is infinite transverse to the settling direction. We present the analogue of the Caffish–Luke argument for diverging velocity fluctuations with side walls present, and find that it predicts the velocity fluctuations should vary across a cell. The consequences of side walls are explored through scaling arguments and numerical simulations. It is argued that at least two different regimes of sedimentation should exist in a box with walls: a weakly interacting regime, where a Caffish–Luke-like law holds, and a strongly interacting regime, where particle interactions modify this behavior. Computer simulations and scaling arguments are presented to explore the strongly interacting regime. It is argued that experiments have not yet completely ruled out the possibility of the divergence of the fluctuations with system size, although if the divergence exists it must be weaker than the Caffish–Luke prediction.

We also present another screening mechanism that should apply to much larger cells or higher particle Reynolds number than those given in current experiments. It is based on the fact that the divergence of velocity fluctuations occurs because of the assumption that momentum diffusion away from test particles is instantaneous. However, if the velocity fluctuations diverge, then the particle diffusivity also diverges (see, for example, Koch¹⁸); eventually, the particle diffusivity will be large enough that particle diffusion beats momentum diffusion. In this limit, it is no longer valid to assume that momentum diffusion is instantaneous, which leads to a self-regulation for the size of fluctuations. Whether the side-wall-dominated or inertia-dominated screening mechanism applies depends on the relative size of the container and the particle Reynolds number.

Finally, it is pointed out that a natural consequence of these arguments is that the fluctuations lead to a *positive* correction to the mean sedimenting velocity, whose form is independent of the screening mechanism. In general, we argue that there is a correction to the mean settling velocity of order $\Delta U/\sqrt{N_{\text{blob}}}$, where ΔU is the size of the fluctuations, and N_{blob} is the number of particles region with correlated velocity field. From the Segre *et al.* experimental data, this implies a leading order $\phi^{1/3}$ correction to the mean velocity. Combined with our suggestion that the saturation mechanism

in the Segre *et al.* experiments is geometry dependent, this leads to the conclusion that the mean sedimenting velocity can depend on the container shape,¹⁹ as previously suggested by Tory *et al.*²⁰

II. STATEMENT OF PROBLEM

Consider a large group of particles falling together in a viscous fluid of infinite extent. Neglecting interparticle interactions, each particle falls according to the Stokes drag law $F = 6\pi\rho\nu U_s a$, where $F = \Delta\rho g v_p$ is the applied force. Here $\Delta\rho$ is the density difference between the particle density and fluid density ρ , ν is the fluid kinematic viscosity, g is the gravitational acceleration, and the particle volume $v_p = 4/3\pi a^3$. The fluid velocity solves the Navier–Stokes equations

$$\rho(\partial_t \mathbf{u} - U_s \partial_z \mathbf{u} + \mathbf{u} \cdot \nabla \mathbf{u}) = \rho \nu \nabla^2 \mathbf{u} - \nabla p + \mathbf{f}, \quad (2)$$

where \mathbf{u} is the fluid velocity relative to $U_s \hat{z}$. The flow is incompressible and the boundary condition is that each particle moves with the fluid. An effective approximation^{4,21} eliminating the boundary condition is to consider the limit of point particles. These are represented by a body force in Eq. (2), of the form $\mathbf{f} = \sum_n f_n \delta(z - z_n) \hat{z}$, with the locations z_n coinciding with the particle positions. Each force f_n is the Archimedian buoyancy force F described above.

We begin with a brief review of the argument developed for computing the average velocity of the suspension^{4,6} in an infinite system: The first step is to neglect the inertial terms in Eq. (2), since the particle Reynolds number Re_p is small. Then, Eq. (2) is averaged over all configurations in which a single test particle is fixed at the spatial location \mathbf{r}_1 .⁶ Denoting this conditional average by an overbar yields

$$\tilde{\nu} \nabla^2 \bar{\mathbf{u}} = \nabla \bar{p}^* + \tilde{F} \hat{z} \delta(\mathbf{r} - \mathbf{r}_1), \quad (3)$$

where $\tilde{\nu}$ and \tilde{F} are the “renormalized” viscosity and force seen by the fixed test particle, representing the average effect of the other particles in the suspension. Detailed computations of $\tilde{\nu}$ and \tilde{F} are described by Batchelor⁴ and Hinch,⁶ the upshot is that both contain $O(\phi)$ corrections to the values for a homogeneous fluid. In deriving Eq. (3), it is necessary to use Batchelor’s renormalization of the pressure $p = p^* + \Delta\rho \nu_p \phi g z$, accounting for the uniform backflow arising from the bottom boundary.⁴ The conclusion of these arguments is that the velocity field surrounding a test particle has the same functional form (decaying as r^{-1} at large distances from the particle) as a particle in a homogeneous fluid, albeit with $O(\phi)$ corrections to coefficients.

This formalism immediately suggests that, for a random suspension, the velocity fluctuations diverge with system size. Caffisch and Luke’s argument⁸ points out that the variance in the velocity fluctuations is given by

$$\langle \mathbf{u}^2 \rangle = \int dP \bar{\mathbf{u}}^2, \quad (4)$$

where dP represents the probability measure for particle positions. If the particle distribution is uniform (implying that in the frame of the mean flow, particles sample their accessible space uniformly) the probability measure is dP

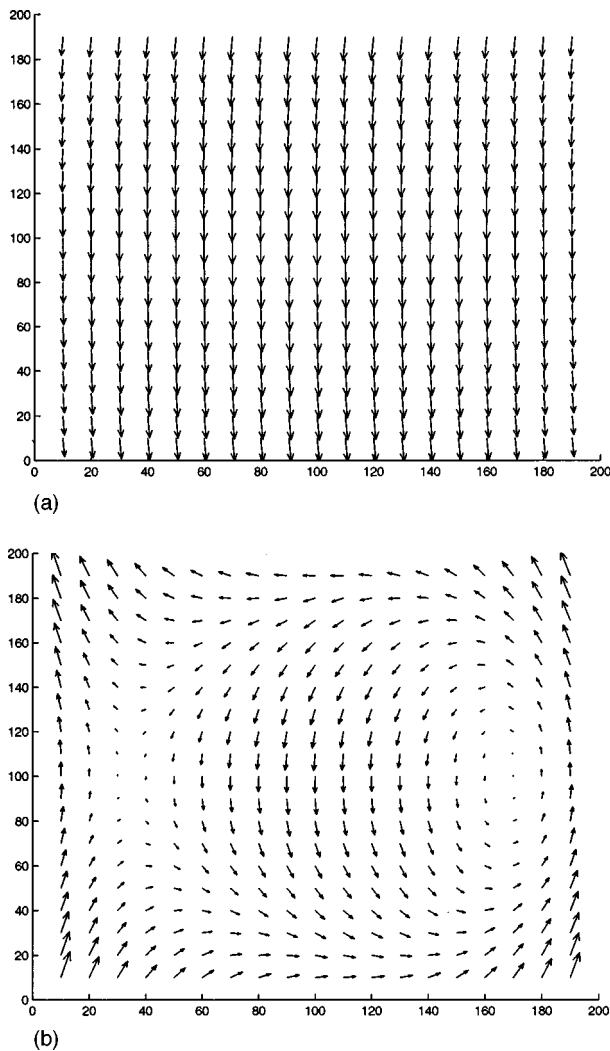


FIG. 1. Visualization of the velocity fluctuations from a random distribution of 10^4 particles. (a) shows the velocity field in the lab frame, and (b) shows the velocity field in the frame moving with the particles. The velocity field was computed using the fundamental solution to Stokes equation in an infinite system (see Sec. III). The large scale swirl that forms in (b) indicates that the velocity fluctuations depend on the system size. The mean particle spacing in this figure is approximately 20.

$= \phi d^3 r / v_p$. Since the solution $\bar{\mathbf{u}} \sim r^{-1}$, as described above, it follows that the integral diverges linearly with system size: $\langle \mathbf{u}^2 \rangle \sim \phi r$.

A more physical version of this argument was given by Segre *et al.*,¹⁵ in the spirit of Hinch:⁹ Consider a blob of size l of fluid. The number of particles in the blob is $N_{\text{blob}} = l^3 \phi / v_p$. Random statistics implies $\sqrt{N_{\text{blob}}}$ fluctuations in the number of particles and hence fluctuations of $\sqrt{N_{\text{blob}} \Delta \rho g v_p}$ in the blob mass. This must balance the Stokes drag $6 \pi \rho \nu l \Delta U$, implying

$$\frac{\Delta U}{U_s} = \sqrt{N_{\text{blob}}} \frac{a}{l} = \sqrt{\frac{3 \phi}{4 \pi}} \sqrt{\frac{l}{a}}. \quad (5)$$

Figure 1 shows a visualization of the divergence: 10 000 particles were placed randomly in a square box with sides of length 200, surrounded by an infinite fluid. Figure 1(a) shows the velocity field produced by these particles (inside the box

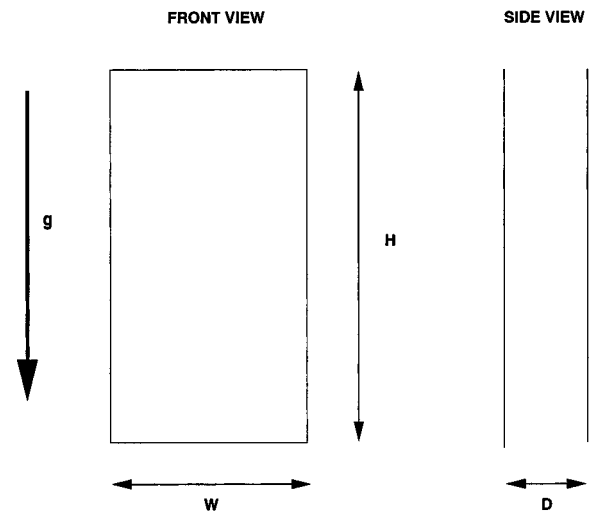


FIG. 2. Sketch of a typical experimental geometry. The thickest arrow represents the falling direction.

containing the particles), and Fig. 1(b) shows the velocity field relative to the mean. The flow relative to the mean is a “swirl” on the scale of the box size. The counterintuitive fact is that the motion of a single particle relative to the mean is *not* controlled by its nearest neighbors, but instead by a collective effect of the entire flow field. In Fig. 1, the mean particle spacing is about 20, which is a factor of 10 smaller than the size of the swirl.

The central argument has been that this divergence in velocity fluctuations for infinite systems (or the dependence of the fluctuations on system size in a finite system) is unphysical, and should be cut off at some scale. That is to say, the “swirls” apparent in Fig. 1 should exist on a scale much smaller than the size of the system. This issue is not just academic: The effective diffusivity in a sedimenting mixture is controlled by the nature of the velocity fluctuations that form.

A screening mechanism is a physical effect which renders integral (4) convergent. There are essentially two possibilities for how this can occur: the first possibility, as proposed by Koch and Shaqfeh,¹⁶ does not change the $\bar{\mathbf{u}} \sim r^{-1}$ law predicted by Eq. (3) but instead relies on a nontrivial particle distribution to force the convergence of the integral. Koch and Shaqfeh demonstrated that this only works for a very special class of particle distribution functions: The distribution of particles around a single test particle must always have a net deficit (compared with a random distribution) of precisely one particle. This screening mechanism is observable in practice only if this special configuration of particles is stable.

The second possibility for screening is to keep the probability distribution essentially random and make $\bar{\mathbf{u}}$ decay faster than r^{-1} . Both of the mechanisms discussed herein are of this latter type.

III. WALL EFFECTS

According to the arguments presented above, the size of the velocity fluctuations diverges for an infinite system, and

is set by the shape of the container for a finite system. There are two different subtleties that are associated with container walls. The first is exposed by the following simple question: Consider a container with width W , depth D , and height H . Which of these scales provides the cutoff for the divergence in the fluctuations? The answer depends on the *boundary conditions* on the fluid velocity field; see Fig. 2.

If the boundaries do not exert forces on the flow field, the divergence is cut off by the *larger* of W , D , and H . The reason for this is that if the $\bar{\mathbf{u}} \sim r^{-1}$ law extends to all boundaries, then the distance to the furthest boundary dominates the far field of the integral. On the other hand, if the boundary conditions on the wall are no-slip, the container walls exert a drag on the particles, and this conclusion is false. Exact solutions demonstrate that close to the wall, the $\bar{\mathbf{u}} \sim r^{-1}$ law changes to a more rapid decay, generally faster than r^{-2} (see below). The consequence of this is that in an actual experiment with rigid walls, the distance to the *nearest* wall provides the cutoff for the fluctuations.

The nature of the decay of the velocity field around a single particle then depends on the shape of the container. For a particle translating parallel to a rigid wall a distance d away, Blake^{22,23} and Lorenz^{24,25} demonstrated that for $r \ll d$, the Stokes solution $\bar{\mathbf{u}} \sim r^{-1}$ holds. However, far enough away, the decay law transitions to $\bar{\mathbf{u}} \sim r^{-2}$. The exact formula for the velocity field is complicated, and contains a superposition of Stokeslets and higher order corrections. A pedagogical description of the details is given in Pozrikidis.²⁵ Exact formulae also exist^{22,24,25} for particles translating perpendicular to a wall; in this case the crossover is from r^{-1} to r^{-3} .

Solutions for point forces moving in the vicinity of boundaries have been tabulated for a number of different geometries; two important geometries for the present discussion are parallel plates^{26,27} and circular cylinders.^{28,29} For parallel plates, Liron and Mochon constructed the solution, which demonstrates²⁶ r^{-2} decay for motion parallel to the plates. Motion perpendicular to the plates decays exponentially in the far field. Liron and Mochon also estimated convergence of the two plate problem to the single plate solution in the limit where the plate spacing becomes infinite, and noted that the influence of the second plate is important when the distance d of the particle from the closest plate is more than $D/8$, where D is the distance between the plates. The circular cylinder differs qualitatively from the examples with plates in that the walls surround the particle on all sides. The qualitative consequence of this is that the walls exert a constant drag force per unit length of the cylinder. Hence, as demonstrated by Blake²⁸ and Liron and Shahar,²⁹ far enough from the point force the velocity field decays exponentially. The crossover between r^{-1} decay and exponential decay occurs at a scale of order the radius of the pipe.

The second subtlety associated with container walls involves the notion^{3,4} that the particle distribution is random and homogeneous. This idea is based on the assumption of ergodicity: In the reference frame falling with the sediment, the particles trajectories are supposed to explore space uniformly. In the presence of side walls and strong particle interactions, this assumption is false. The reason is that side

walls make the velocity fluctuations, and hence the particle diffusivity, depend on the distance between the particle and the wall. The no-slip boundary condition requires that the diffusivity vanishes at a wall, so that the diffusivity reaches a maximum on the midplane of the cell. The consequence of a nonuniform diffusivity is that a collection of particles initially uniformly distributed in the cell will migrate toward the side walls. This assertion will be demonstrated through a computer simulation of a model sediment in the next section.

The nonuniformity of the velocity fluctuations in a random sediment follows directly from formula (4), except using the correct Green's function for a particle in a cell with solid boundaries:

$$\Delta U^2(\mathbf{r})_{UB} = \phi I = \phi \int_{\text{cell}} \mathbf{u}(\mathbf{r} - \mathbf{r}')_{\text{cell}}^2 \frac{d^3 r'}{v_p}. \quad (6)$$

Here, \mathbf{u}_{cell} is the velocity field of a single particle in the cell, and the integral is over the entire cell. As discussed above, since \mathbf{u}_{cell} decays at least as fast as r^{-2} asymptotically, this integral converges. However, the value of the integral depends on the location of \mathbf{r} in the cell, and in particular on the distance from a side wall. When sampled at a wall, $\mathbf{u} = 0$ so the fluctuations vanish; ΔU is maximum in the center of the cell. Since in general $\mathbf{u}_{\text{cell}} \sim U_s a r^{-1}$ for $r < O(d)$ (if d is the distance from the particle to the nearest container wall), this integral will in general be $I = c U_s^2 d/a$. The constant c is a geometrical factor, and can be much larger than unity (c.f. in the planar case, where the transition to r^{-2} behavior occurs at $12d$). Estimates for c in a random suspension as a function of distance from a single wall is given in Appendix A.

The physical reason for the dependence of the size of the velocity fluctuations in a random suspension with distance across the cell is that particles closer to the wall interact with fewer other particles than particles in the center of the cell. In particular, at a distance x from the wall of a cell, a particle interacts via the $\mathbf{u} \sim r^{-1}$ law with $N(x) = \phi x^3/v_p$ particles, where ϕ is the local volume fraction. The fluctuations about this number lead to a particle excess or deficit of $\pm \sqrt{N(x)} \sim \sqrt{\phi x^3/v_p}$ particles, which leads to a fluctuation of size $\Delta U(x) \sim \pm (6\pi\rho v x)^{-1} \sqrt{N(x)} \Delta \rho g v_p$. Hence,

$$\Delta U(x) \sim U_s \sqrt{\phi} \sqrt{\frac{x}{a}}. \quad (7)$$

Therefore, in a random suspension fluctuations should vary with distance to the wall with via a \sqrt{x} law. Any deviation to this formula measured in an experiment would reflect a non-uniformity in the particle distribution across a cell. A conceptually useful way of expressing the formula for the fluctuations is to express

$$\frac{\Delta U^2(x)}{U_s^2} \sim \phi \frac{cx}{a} = \phi \left(\frac{V_0(x)}{v_p} \right)^{1/3}.$$

$V_0(x) = x^3$ is the *interaction volume* of a particle a distance x from the wall—the volume of space around a single particle where the $\mathbf{u} \sim r^{-1}$ law holds.

The notion of interaction volume immediately suggests that there should be at least two different regimes for the velocity fluctuations in a finite cell. Cartoons of the two re-

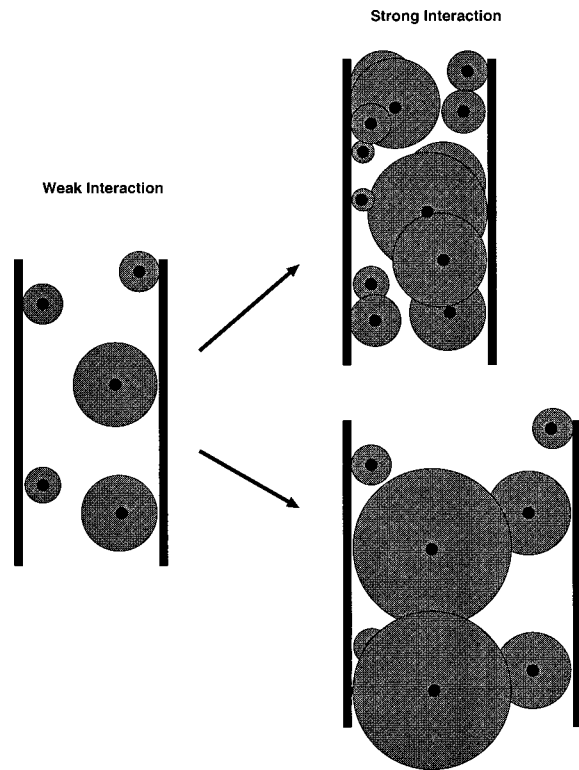


FIG. 3. Cartoons of the weakly interacting and strongly interacting regimes of sedimentation. Around every particle (small dark circles) is the sphere denoting the interaction volume of that particle; within this sphere the particle interacts with other particles via the $u \sim r^{-1}$ law. In the weakly interacting regime, the interaction volumes around different particles (defined to be the volume of space where the $u \sim r^{-1}$ law holds) do not overlap. In the strongly interacting regime, the interaction volumes overlap significantly. A transition from weakly interacting to strongly interacting occurs when either increasing the number density of particles at fixed gap width (top figure) or increasing the gap width at fixed number density (bottom figure).

gimes are depicted in Fig. 3. Around each particle, we have drawn a circle with radius the distance of the particle to the wall, depicting the interaction volume for this particle. Inside of this volume, the particle interacts strongly (i.e., by the $u \sim r^{-1}$ law) and outside the volume the interactions are weaker. In the *weakly interacting regime* [Fig. 3(a)] the interaction volumes surrounding different particles do not overlap. In the *strongly interacting regime* [Fig. 3(b)] the interaction volumes of different particles overlap significantly.

In the weakly interacting regime, particles interact with each other with velocity laws which decay much faster than r^{-1} . In principle, what happens in this case could depend on the cell geometry, since different cells have different interaction laws. However, the simplest expectation is that an initially random distribution of particle distribution remains random for all times. This would lead to a dependence of fluctuations on ϕ and system size that is directly predicted by Eq. (6): Namely, $\Delta U/U_s = c(W/a)\sqrt{\phi}\sqrt{D/a}$, where the constant c is geometry dependent. In the limit of low volume fractions, the $\sqrt{\phi}$ law must be obeyed, because the time scale of interactions between different particles grows significantly: for example, in Appendix B it is shown that the exact solution of Liron and Mochon²⁶ implies that, for two par-

ticles falling between two plates, the time scale for motion perpendicular to the plates grows exponentially with their separation distance ρ parallel to the plates, when $\rho > D/2$.

In the strongly interacting regime, what happens depends on the result of particle interactions. In this regime the non-uniformity in ΔU across the cell implies that the particle flux toward the side walls is strongest in the center of the cell, so that over time the center of the cell will be depleted of particles. Heuristically, the side walls are kinetic traps for particles, since once a particle diffuses toward a wall it takes increasingly long for it to escape. Simulations described below confirm this conclusion. The consequence of particles being pushed away from the center of the cell is that the typical size of the velocity fluctuations in the strongly interacting regime will be *smaller* than that predicted by Eq. (6).

When is the transition between the weakly and strongly interacting regime? At fixed volume fraction ϕ , the transition from weakly to strongly interacting occurs by increasing the distance D between the walls. Hence, there is a critical distance D_{crit} (for fixed ϕ) or alternatively a critical volume fraction ϕ_{crit} (for fixed D) above which particle interactions can strongly modify the fluctuations from that of a random distribution. A lower bound for ϕ_{crit} is that the particles fall “single file” through the cell, occurring at $\phi_* = (2a/D)^3$.

Before proceeding with numerical simulations to test these ideas, we first analyze the *maximum* size of a blob that can occur in a cell of depth D (with $W \gg D$) that behaves precisely like a blob in an infinite system. Each of the particles in such a blob must interact with each other via a $u \sim r^{-1}$ law. This requires that every particle in the blob is closer to the others in the blob than to its nearest wall. The maximum blob for which this constraint holds is centered on the midplane between the two side walls, and has size $D/3$ in the direction along the depth, and a size $D/2$ along the width and the height. Any blob which is larger than this bound necessarily has some of its particles interacting more weakly than they would in the infinite system limit. It should be emphasized that these bounds follow directly from the properties of the single particle Green’s functions to Stokes equation, and have nothing to do with complications that occur when many particles interact.

A. Numerical simulations of a model sediment

To substantiate the effect of wall interactions, this subsection presents numerical simulations of a model sediment confined between two infinite rigid walls. We will assume, as above, that the particle Reynolds number ($U_s a/\nu$) is small so that the fluid velocity solves the Stokes equations. We are interested in the dynamics at very low particle volume fractions, where the average interparticle spacing is much larger than a particle size. In this limit, it is appropriate to consider the limit of point particles, each of which exerts a localized force on the fluid.

1. Formulation of model sediment

Denoting the particle positions by \mathbf{x}_n , the equations of motion are

$$\frac{d\mathbf{x}_n}{dt} = \mathbf{U}_n + (6\pi\mu a)^{-1}\mathbf{f}, \tag{8}$$

$$\mathbf{U}_n = \sum_{i \neq n} \mathbf{S}(\mathbf{x}_i; \mathbf{x}_n) (6\pi\mu a)^{-1}\mathbf{f}. \tag{9}$$

Here, \mathbf{U}_n is the velocity of the fluid at the location of the n th particle if this particle were absent, $\mathbf{f} = 6\pi\mu a U_s \hat{z}$ is the localized force each particle exerts on the fluid, and $\mathbf{S}(\mathbf{x}_i, \mathbf{x})$ represents the Green's function of the Stokes equation for a point force located at \mathbf{x}_i , obeying the appropriate boundary conditions at the side walls. Formula (8) is a consequence of Faxen's first law,⁵ which states that a particle sitting in a flow \mathbf{U}_n and feeling a force \mathbf{f} moves as the sum of the Stokes velocity $(6\pi\mu a)^{-1}\mathbf{f}$ and \mathbf{U}_n . Given a formula for the Green's function \mathbf{S} these equations solve for both the position and velocities of the particles in the sediment.

To proceed with simulations of a sediment trapped between two infinite plates (located at $x = 0$ and $x = L$) we need an approximation for the Green's function \mathbf{S} obeying the boundary conditions. We seek an approximate formula for \mathbf{S} with three important features: (1) It must have the correct near-field asymptotics, i.e., r^{-1} decay closer to the particle than the nearest wall; (2) It must have the correct r^{-2} decay law on scales farther from the particle than the nearest wall; and finally (3) It must exactly satisfy the correct boundary conditions on the plates. This last property is especially crucial because the major point of these simulations is to investigate the consequences of a vanishing diffusivity near the particle walls.

There are several different approaches that could be followed for finding \mathbf{S} . In the point particle limit, the solution for a particle falling between two walls can be represented as a infinite sum of image Stokeslets (reflecting the particle positions about the two walls), plus a correction. The correction is necessary because, although the sum of image Stokeslets lead to a vanishing velocity parallel to the walls, the component of the velocity perpendicular to the walls does not vanish. Liron and Mochon²⁶ found the correction by expressing the sum of image Stokeslets in terms of an infinite series of Bessel functions, and solving for the correction in each mode explicitly. One possibility is to use a truncation of this series solution as an approximation for \mathbf{S} , as it converges very rapidly farther from the particle than the wall spacing. However, the convergence of this series is very slow in the near field, closer to the particle than the wall spacing. The alternative idea of basing a numerical method on the sum of image stokeslets has the defect that the convergence is very slow in the far field. [The best way to do this calculation is to compute the Green's function numerically and then use a lookup table for efficiently simulating the particle dynamics (H. Stone, private communication). This is planned for a future work.]

For the present simulations, we chose a balance of opposing evils which is both computationally efficient and respects important features mentioned above. Denoting $\mathbf{S}_p(\mathbf{x}, \mathbf{x}')$ the Stokeslet for a single particle in an infinite medium for a particle located at \mathbf{x}' , the formula for \mathbf{S} that we use is

$$\mathbf{S}(\mathbf{x}, \mathbf{x}') = \sum_{n=-N}^N (\mathbf{S}_p(\mathbf{x}, \mathbf{r}_n) - \mathbf{S}_p(\mathbf{x}, \mathbf{R}_n)) \gamma(x), \tag{10}$$

where $\mathbf{r}_n = (x' - 2nD, y', z')$ and $\mathbf{R}_n = (-x' + 2nD, y', z')$. The function $\gamma(x) = 1$ for the components of \mathbf{S} parallel to the side walls, and $\gamma(x) = \sin(\pi x/D)$ for the \hat{x} component of \mathbf{S} . This ensures that the boundary conditions on the walls are obeyed exactly for all components of \mathbf{S} , while respecting the symmetries of \mathbf{S} with respect to interchange of \mathbf{x} and \mathbf{x}' . (See Appendix B for a discussion of this point.) The number of image Stokeslets N taken in the sum is chosen independently for each simulation: in particular, we verify that N is large enough that the numerical results converge and are independent of N . Typically in the simulations that follow this requires keeping $N \approx 10$. In writing the explicit formula for \mathbf{S} we will nondimensionalize all length scales by a and all timescales by aU_s^{-1} .

Another subtlety that needs to be addressed is that the single particle Stokeslet

$$\mathbf{S}_p = \frac{1}{8\pi} \left(\frac{1}{|\mathbf{r}|} + \frac{\mathbf{r}\mathbf{r}}{|\mathbf{r}|^3} \right)$$

has a singularity at $\mathbf{r} = (x, y, z) = (0, 0, 0)$. Hence, if a pair of particles in the simulation happen to overlap, the settling velocity predicted by Eq. (8) will be unrealistically large due to the large velocity induced by each particle on the other. This effect could produce large spurious effects on the velocity fluctuations in a simulation. Previous studies have avoided this problem by either using a more accurate representation of the hydrodynamic forces than the point particle approximation allows,³⁰ or by including a short ranged repulsive force between the particles.³¹ Here, we will simply cut off the divergence of the single particle Stokeslet by modifying it to be

$$\mathbf{S}_p = \frac{1}{8\pi} \left(\frac{1}{\tilde{r}} + \frac{\mathbf{r}\mathbf{r}}{\tilde{r}^3} \right), \tag{11}$$

where $\tilde{r} = (x^2 + y^2 + z^2 + 1)^{1/2}$. This cuts off the unphysical divergence while maintaining the important asymptotic properties mentioned above. Also, two overlapping particles move at exactly twice the velocity of a single particle, which is essentially correct. It should be remarked that this cutoff of the Stokeslet divergence is the only place that the particle size enters explicitly into the formula for \mathbf{S} .

The last element of the simulations is that we need to correct the particle mobility due to the presence of the side walls: Particles near walls fall more slowly than particles in the center of the cell. We account for this by taking the particle velocity to be $\mathbf{U} = (6\pi\rho\nu a)^{-1}\mathbf{f}\psi(x)$, where $\psi(x) = 1 - a(2l)^{-1}$ with l the distance of the particle to the closest wall.

We emphasize that this formulation is a *model* for the motion of the particles in the presence of walls, utilizing several approximations which are physically reasonable but not necessarily mathematically well controlled. [The most egregious approximation in the model is $\gamma(x)$, which implies

that the velocity field is not divergence free. In principle this could lead to systematic errors in computed probability distributions across the cell.]

The goal of the calculations is to show the qualitative effect of walls on the particle motion. Quantitative comparisons between numerical results and experiments requires a more accurate representation of the Green's function.

2. Blob breakup

The physical argument for computing the size of the fluctuations in an infinite system relied on the dynamics of "blobs," i.e., regions of particle density higher or lower than average. In an infinite homogeneous system, a group of particles clumped together in a spherical clump fall together in a spherical clump for long times. Evidence for this long time coherence is given by Nitsche and Batchelor³¹ in a numerical simulation of a falling blob. The simulation demonstrates that particles shed from the blob extremely slowly: e.g., their simulation demonstrates that in a time of order $200aU_s^{-1}$ only about 1% of the particles escape from the blob.

The lifetime of a blob is important in understanding the size of the velocity fluctuations during sedimentation; blobs are constantly being created and destroyed, and the size to which they can grow depends on how long they survive. To understand how the presence of container walls modifies this conclusion, we simulate the evolution of an initially random distribution of particles between two walls. The initial distribution is finite, and surrounded by clear fluid. Figure 4 shows a simulation of the dynamics of 100 particles confined in a gap of width $10a$. The initial distribution of particles is random, filling the gap as well as a region of size $20a \times 20a$, so the initial volume fraction is $\phi_0 \approx 0.01$. The different rows represent snapshots at $t = 15, 30, 100,$ and 200 , respectively (in units of aU_s^{-1}). The arrows represent the magnitude of the velocity field in the laboratory frame. The left column shows the particle distribution perpendicular to the plane of the walls; the velocity field is evaluated on the midplane of the cell, halfway between the two walls. The right column shows the evolution within the thin gap, with the velocity field evaluated at $y = 10$.

There are several important features that should be noted from this simulation, which differentiate the evolution of a "blob" in a confined geometry from that of an infinite system:

(1) Particles in the center of the cell (near the midplane) move faster because they have a larger interaction volume and thus are able to interact with more particles. This causes a "stretching" of the initial blob: After a time $30aU_s^{-1}$, the extent of the blob in the vertical direction has nearly tripled. In contrast, the simulation of Nitsche and Batchelor³¹ shows that (in the absence of walls) the blob size stays roughly constant during this time.

(2) There is a swirling motion of the particles in the gap between the two walls. This can be most easily seen through an animated movie of the blob disintegrating (which unfortunately cannot be included in this paper). Another indication is shown in Fig. 5, which plots a typical particle path falling through the cell. The particle moves back and forth across

the smallest dimension of the cell. At long times, the particle stops at the right wall.

In fact, essentially every particle in our simulation eventually ends up stuck to the side walls. The reason for this is partly an artifact of our simulation procedure, and partly a reflection of the actual dynamics: on one hand, we make no attempt to accurately model lubrication forces when a particle approaches a wall, so that the evolution of the particle dynamics near the wall is incorrect. On the other hand, Appendix B shows that for *two particle* interactions, when the particles are sufficiently far from each other (of order $D/2$) in the direction parallel to the wall generically one of the particles will segregate to the wall. Hence, there is an overall tendency for particles to force each other toward the wall, although the details of what happens when the particle approaches the wall are not well accounted for here.

(3) The maximal fluctuations in this cell are localized three dimensional "blobs," in spite of the fact that the initial distribution of particles had a size much larger than the gap width. Hence, the presence of a thin gap does *not* make the system sediment two dimensionally. Evidence for this assertion is shown in Fig. 6, which show a "front view" of the flow field around the group of particles in the above simulation which results in the maximal velocity at $t = 10$. The radius of this group of 25 particles is of order $5a$; the flow field is very similar to that of the same blob falling in an infinite three dimensional fluid: The measured falling velocity of the group of particles is $\approx 4.5U_s$, whereas the predicted velocity for a blob of N particles and radius R surrounded by an infinite fluid is $N(a/R)U_s = 4.8U_s$.

(4) Correspondingly, the magnitude and nature of the fluctuations in the simulation depends on the gap width D . To illustrate this, Fig. 7 shows the maximal velocity fluctuation at $t = 10$ in a simulation with the same initial volume fraction as that of Fig. 6, but with double the gap width $D = 20a$. The maximal fluctuation is a blob of 54 particles with radius ≈ 7 .

(5) Particles near a wall have a much smaller fluctuation velocity than a particle in the center of the cell. Because of this, it takes much longer for a particle near the wall to move to the center of the cell than for a particle in the center of the cell to move to a wall. At long times this results in segregation of particles to the walls. We believe that in a continuously fed sediment, this process must reach a steady state: When the particle density near the wall increases, the fluctuations there will also increase. Eventually the fluctuations near the wall will be of order that in the center of the cell, and the system will reach a steady state. Our simulations are not able to currently capture this steady state because of both our inadequate modeling of the particle-wall interaction and the fact that we use too few particles.

B. Comparison with previous experiments

We now re-examine previous experiments with wall effects in mind. From this viewpoint, the two types of experiments that have been performed to date represent very different measurements. The particle tracking algorithm of Ham and Homsy¹² and Nicolai and Guazzelli^{13,14} follow a single

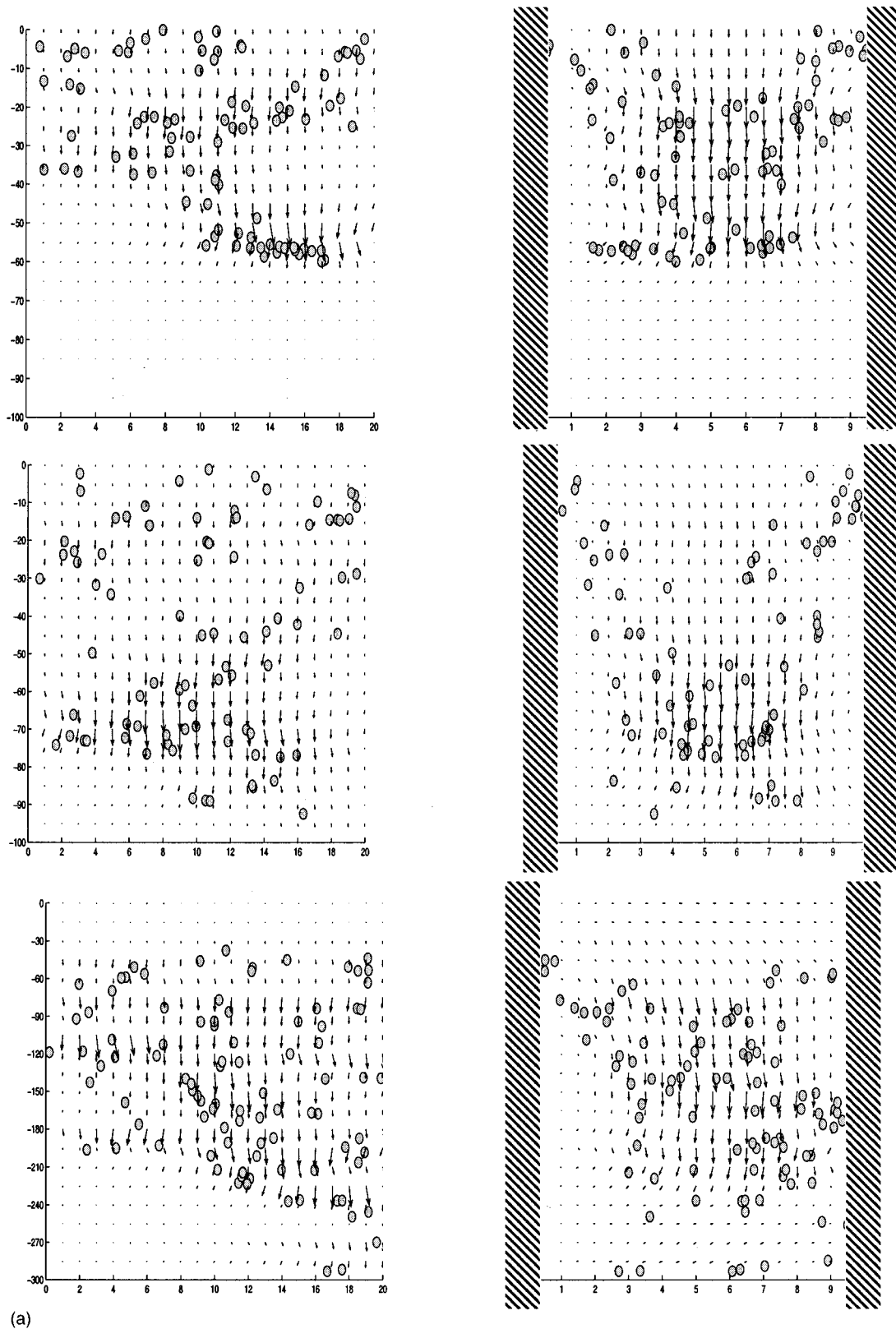


FIG. 4. Snapshots of the simulation of the falling blob. Successive rows show times 15, 30, 100, and 200 in units of aU_s^{-1} . The left column represents a front view, looking down on the sediment perpendicular to the walls. The right column represents a side view, with the walls (hatched regions) located at $x=0$ and $x=10$. The velocity vectors show the relative magnitudes of the velocity field produced by the particle distribution, according to our approximate Green's function S . For the left column the velocity field is evaluated at the midplane of the cell; for the right column the velocity field is evaluated at $y=10$, the initial midplane of the blob. Note that the scales on the plot in the z direction differ in the different frames.

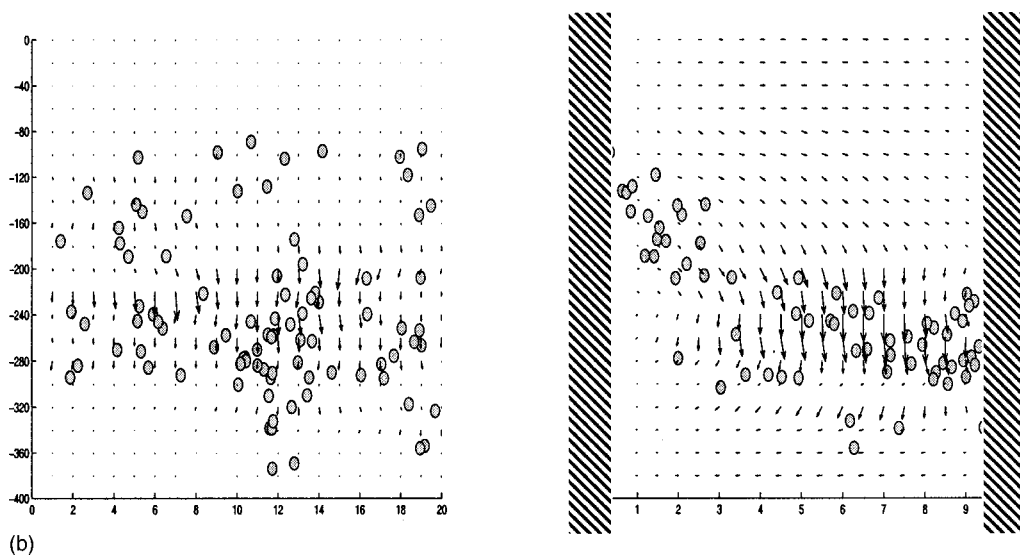


Fig. 4(b) (Continued.)

marked particle in its path through the cell. If we assume that the particle distribution is essentially random, then particles spend longer near walls; the fluctuations near the walls will then dominate the long time average. On the other hand the Segré *et al.* experiments measure the velocity field at fixed time on the *midplane* of the cell, where the fluctuations should be maximal.

The Segré *et al.* experiments consider both rectangular cells with $W \times D$ varying from $3 \text{ mm} \times 0.3 \text{ mm}$ to $30 \text{ mm} \times 10 \text{ mm}$, and a 0.5 mm radius cylinder. Most of the data obeying the $\Delta U \sim \phi^{1/3}$ scaling laws have $10 \text{ mm} \times 1 \text{ mm}$ cells. The experiments image the velocity field in the median plane of the cell with a depth of field of approximately $\pm 0.5 \text{ mm}$. On increasing the cell width W the correlation length

saturation; the surprising feature of this measurement is that the saturation occurs with the *largest* dimension transverse to the falling direction, contradicting simple expectations outlined above for an experiment with rigid walls. Moreover, the measured correlation lengths show a nontrivial volume fraction dependence $l \approx 30a\phi^{-1/3}$.

The observed correlation lengths vary between 1 mm and 5 mm , and are always *larger* than the distance to the closest walls $D/2$. As an example, the particle image velocimetry images in Fig. 1 of Segré *et al.* have cell half-depths of $D/2 = 1 \text{ mm}$ for the $\phi = 10^{-4}$ data, and $D/2 = 0.5 \text{ mm}$ for the $\phi = 0.03$ data. The measured correlation lengths (in the directions parallel to the nearest plates) are on the order of 4 mm and 1 mm , respectively. This means that the walls must be affecting the results. However, the reported dependence on volume fraction gives $\Delta U \sim U_s \phi^{1/3}$, which differs from

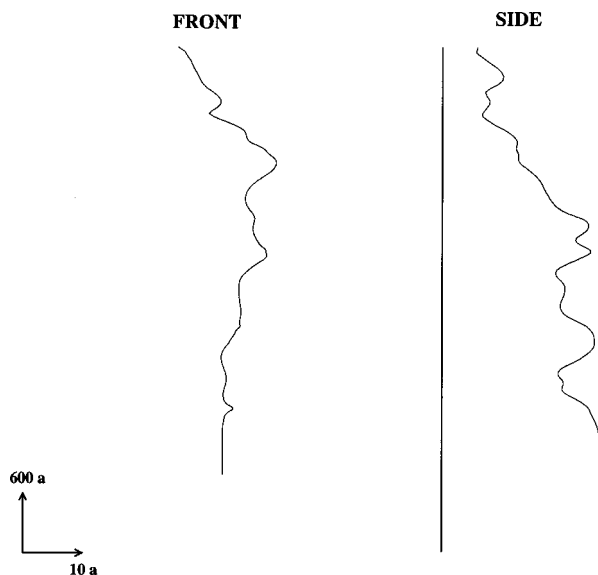


FIG. 5. Top and side view of a particle path in the blob disintegration simulation shown above. The scales in the y and x direction are the same ($10a$), whereas the scale in the falling z direction is compressed. Note that the fluctuations in the trajectory in the plane perpendicular to the side walls is of the order of the fluctuations in the trajectory between the walls.

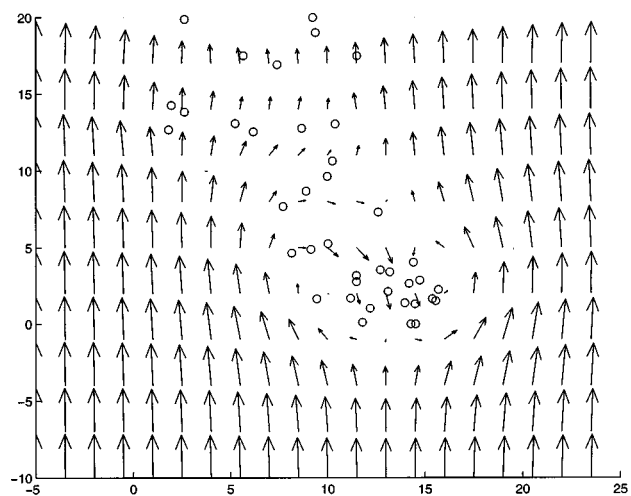


FIG. 6. Closeup of the particles falling the fastest in the above simulation (front view). Twenty-four particles are clumped in a "blob," of radius approximately $5a \sim D/2$. The falling velocity of this blob is measured to be $\approx 4.5U_s$, which is close to the prediction $N(a/R)U_s = 4.8U_s$ for a three dimensional blob.

the volume fraction dependence of the weakly interacting regime. The $\Delta U \sim U_s \phi^{1/3}$ law occurs for the data where there is no dependence of velocity fluctuations on system width W . This implies that for these data, an additional dynamical process must occur in the experiments.

We hypothesize that the dynamical effect is particle motion toward the walls. As shown above, fluctuations make a particle initially on the center line of the plate (in the imaging window) move off the center line because of a component ΔU of its velocity directed toward the wall. As emphasized above, this limits the size of the fluctuations that can form in this system as it limits the number of particles that can participate in a correlated velocity fluctuation; see Fig. 8.

We now present a scaling argument incorporating this physical idea, which reproduces the scaling laws measured by Segré *et al.* By dimensional analysis, a particle initially on the center plane will reach the wall after a time $\tau \sim D/2\Delta U^{-1}$, where ΔU is the characteristic size of the velocity fluctuations transverse to the walls. [We remark that sedimentation is unlike the “blob disintegration” calculation shown above because the characteristic blob size (which determines ΔU) is set dynamically.] At this point, the velocity field around the particle no longer decays like r^{-1} and thus does not affect many other particles. As demonstrated by the simulations of the preceding section, the particle no longer participates in a correlated velocity fluctuation with other particles. Hence, τ is the correlation time. The distance the particle falls during this process is of order

$$l \sim U_s \tau = \frac{D}{2} \frac{U_s}{\Delta U}. \tag{12}$$

This distance represents the maximum size of a region of correlated velocities that can form in this experimental ge-

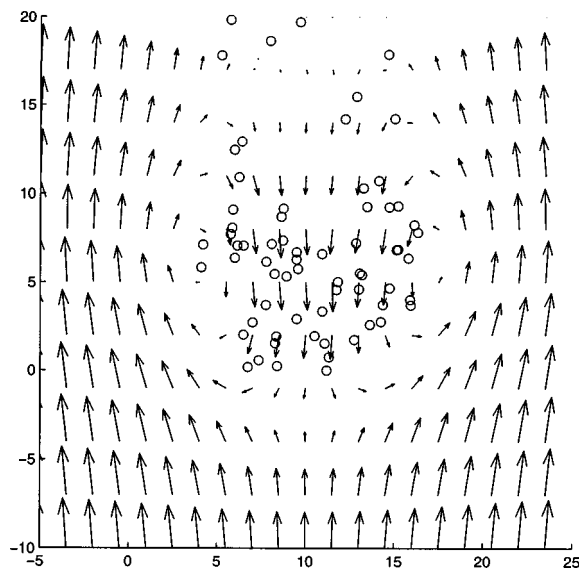


FIG. 7. Closeup of the particles falling the fastest in a simulation with $D = 20a$, but with the same initial volume fraction as that of Fig. 6. Fifty-four particles are clumped in a “blob,” of radius approximately $7a \sim D/2$. The falling velocity of this blob is measured to be $\approx 8.2U_s$, which is close to the prediction $N(a/R)U_s = 7.7U_s$ for a three dimensional blob.

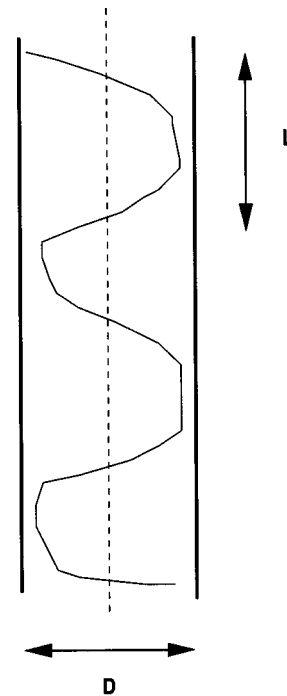


FIG. 8. Side view of thin experimental cell. The dotted lines denotes the center line, which is where the image plane is located in the Segré *et al.* experiments. The thin solid line represents the proposed particle path.

ometry: A larger “blob” does not have time to form without different parts of the blob becoming uncorrelated.

To determine the ϕ dependence of l and ΔU , we need to combine formula (12) with an estimate with the Caffisch and Luke result Eq. (5) for how ΔU depends on the size and number of particles in a correlated region. The combined result is

$$l \sim a(D/2a)^{2/3} \phi^{-1/3}, \tag{13}$$

$$\frac{\Delta U}{U_s} \sim (D/2a)^{1/3} \phi^{1/3}, \tag{14}$$

$$N_{\text{blob}} \sim \left(\frac{D}{2a}\right)^2. \tag{15}$$

The Segré *et al.* experiments¹⁵ operate with a single particle size ($7.8 \mu\text{m}$) and a range of cell sizes. The data for ΔU are mainly taken with $D = 1 \text{ mm}$ cells, so that $D/2a \approx 64$. This implies $N_{\text{blob}} \sim 4100$, $l \sim 17a \phi^{-1/3}$, and $\Delta U \sim 4U_s \phi^{1/3}$, in good agreement with the experiments, for which $N_{\text{blob}} = 3000$, $l_{\parallel} \approx 11a \phi^{-1/3}$, and $\Delta U_{\parallel} \approx 2U_s \phi^{1/3}$. (Here l_{\parallel} and ΔU_{\parallel} denote the correlation length and velocity fluctuation along the sedimenting direction.)

It therefore follows that particle motion controlled by the gap thickness D can lead to scaling laws which are consistent with those measured by Segré *et al.* However, the present author wishes to make no secret of the fact that these scaling laws equations [(12)–(14)] were derived to reproduce experimental findings which were known to the author at the time of the derivation. Therefore, they do not in any way represent a “first principles” theory. The substantive conclusion which should be drawn from the scaling analysis is that the

experiments are *consistent* with dynamics controlled by the gap thickness. Moreover, this conclusion is consistent with the simulations described above, which also suggests that the dynamics should be influenced by the gap.

The seriousness of this conclusion is that both our general arguments and formula (13) imply that the size of the velocity fluctuations is still controlled by the size of the cell. The growth of fluctuations with system size is weaker than that implied by the Caflish–Luke prediction [Eq. (5)] although it still diverges with increasing D . Although it is not possible to directly test the form of this divergence quantitatively with our current simulations, we have verified the qualitative dependence on D and ϕ : On increasing D keeping ϕ_0 fixed, the size of the velocity fluctuations increase; similarly on increasing ϕ_0 keeping D fixed the fluctuations increase.

The scaling laws in Eqs. (12)–(14) will only be valid when the assumption that the three dimensional law $\Delta U \sim \sqrt{N_{\text{blob}}}/l$ applies to the fluctuations is valid; if the size of the blob is large enough relative to the cell size, wall drag will limit the size of the fluctuations. The crossover between these regimes occurs when the velocity fluctuations implied by Eq. (13) is of order the upper bound implied by Eq. (6). Setting ΔU from Eq. (14) to be of order, the upper bound implies a transition at the critical volume fraction

$$\phi_{\text{crit}} \sim \frac{2}{c^6} \frac{a}{D} = \phi_* \left(\frac{D}{2a} \right)^2, \quad (16)$$

where ϕ_* is the volume fraction based on a single particle per interaction volume. This formula has the physical interpretation that when the volume fraction is small enough that fewer than N_{blob} particles exist in an interaction volume, the particle dynamics cannot be described by formulas (12)–(13). As described in the previous subsection, above this threshold the particle interactions are weak and hence the $\Delta U \sim U_s \sqrt{\phi}$ law should hold.

A rough estimate for the critical volume fraction is obtained in Appendix A, which computes the upper bound for a particle is a distance h from a single wall, ignoring all other walls. Applying this formula for experiments with $D/(2a) = 50$ implies $\phi_{\text{crit}} \sim 5 \times 10^{-6}$. As discussed in Appendix A, this estimate overestimates the true answer, and hence this critical volume fraction far underestimates for the correct ϕ_{crit} [note the c^6 power in Eq. (16)]. Taking into account all of the side walls in the cell will decrease the interaction volume.

Since we do not have the Green's function for all experimental geometries, it is not possible to use this argument to compute ϕ_{crit} for realistic experimental geometries. In the Segré *et al.* experiments, the ratio D/a is smallest in the 3 mm \times 0.3 mm cell and the 0.5 mm cylindrical cells, so these are the most likely candidates for being in the $\sqrt{\phi}$ regime. (It is also true that for these two cells the imaging window spans the entire width of the cell, which implies that both sets of walls are probably important for the particles being sampled. This will further decrease the interaction volume, and hence increase ϕ_{crit} for these cells.) With this in mind, we consider the scaling of fluctuations with changing

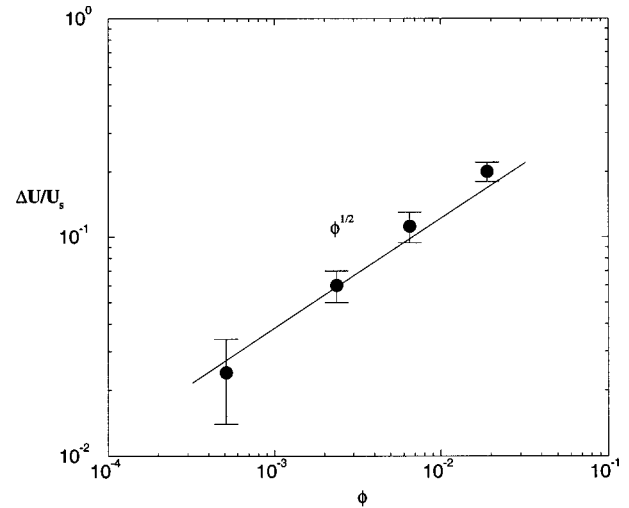


FIG. 9. Replotting of the data from Segré *et al.* for the 3 mm \times 0.3 mm cell, considering it as the dependence of fluctuations on volume fraction instead of system size dependence. The solid lines denotes the $\Delta U/U_s \sim \sqrt{\phi}$ law.

system size W measured by Segré *et al.* Examining Fig. 4 of Segré *et al.* for the size of the fluctuations as a function of system size W , the data naturally separate into two different categories: The *saturated* data (where the velocity fluctuations are independent of W) occur for the cell sizes 10 mm \times 1 mm, 20 mm \times 2 mm, and 30 mm \times 10 mm. The scaling laws for the velocity fluctuations and correlation lengths discussed above in Eqs. (13), (14), and (15) all referred to the cells in the saturated regime. On the other hand, the data which show an increase in the velocity fluctuations with increasing W are for the 3 mm \times 0.3 mm cell and the 0.5 mm round cell.

This suggests the interpretation that these smaller cells have fewer than N_{blob} particles per interaction volume, and hence their velocity fluctuations obey $\Delta U \sim \sqrt{\phi}$. If $\Delta U/U_s \sim \sqrt{\phi}$, then when $\Delta U/\phi^{1/3}$ is plotted against $W/a\phi^{1/3}$, the graph will have positive slope, so that it will appear that the fluctuations are increasing with system size. To test this hypothesis, Fig. 9 replots the data for 3 mm \times 0.3 mm cells from Fig. 4 of Ref. 15 as $\Delta U/U_s$ vs ϕ . It is seen that the data are consistent with the $\Delta U/U_s \sim \sqrt{\phi}$ law. Hence, the proposal that the data consist of two different regimes (with different scaling laws for ΔU) is a consistent interpretation of the data.

The other major set of experiments is by Nicolai and Guazzelli,¹³ who use a very different procedure: instead of the “Eulerian” procedure of Segré *et al.* they follow the paths of single particles meandering through the cell. From these data, they extract the effective diffusion constant. The imaging procedure projects the position of the particle onto a two dimensional plane perpendicular to the thinnest direction of the cell. Since the depth of field in the experiments is the depth of the cell,¹³ no information is obtained about where the particles are located relative to the walls parallel to the imaging window. Although the cells used by Nicolai and Guazzelli are larger than those of the Segré *et al.* experiments (dimensions ranging from $D \times W = 20\text{mm} \times 100\text{mm}$ to $80\text{mm} \times 100\text{mm}$), their particle sizes are also correspond-

ingly larger (394 μm radius spheres), so that their ratio of the smallest cell dimension to particle size ranges from $D/2a = 25 \rightarrow 100$, in precisely the same range as that of Ref. 15.

We now compare the ideas formulated above to the measurements of Nicolai and Guazzelli.¹⁴ The above argument suggested that the correlation time should be $D/2\Delta U^{-1} = a/U_s(D/2a)^{2/3}/\phi^{1/3}$. Comparing with Nicolai and Guazzelli's values for cells ranging from $D = 20\text{ mm} \rightarrow 80\text{ mm}$ implies predictions $\tau \sim 23aU_s^{-1} \rightarrow 58aU_s^{-1}$. In contrast, the measured value is about $17aU_s^{-1}$ for all the cells.

The independence of τ on the smallest scale of the container is a contradiction between the experiment and the theoretical ideas presented herein. There are several possible reasons for this discrepancy:

(1) The argument posed above implicitly assumes that only one set of walls is important and hence that the aspect ratio of the cell is large. Most of the Segré *et al.* experiments have $W/D = 10$, whereas the Nicolai and Guazzelli¹⁴ experiment varies from $W/D = 5 \rightarrow 1.25$. When the interaction volume is limited by both sets of particle walls the prefactors in the scaling laws will depend on both dimensions transverse to the settling.

(2) The ratio of cell size to mean particle spacing $D/(a\phi^{-1/3})$ is larger by about a factor of 5 in the Nicolai–Guazzelli experiment than in those of Segré *et al.* In principle there could be transitions in the flow as this dimensionless parameter increases.

(3) Finally, and most importantly, the presence of side walls can cloud the interpretation of diffusivities extracted from single particle measurements. As emphasized above, for a random suspension, ΔU (and hence the particle diffusivity) is not homogeneous across the cell. However, the measured diffusion constant from single particle tracking reflects an *average* of the diffusivity over the path of the particle. In the experiments, particle paths do not include information about the distance from a particle to its nearest wall; hence, the measured diffusivities reflect a trajectory average over the cell thickness. Since the particle will spend more time closer to a wall, where the fluctuations are smallest, this average weights smaller fluctuations more than larger ones.

To illustrate the effect of this averaging, we analyze a typical particle trajectory in the blob disintegration simulations. This is not equivalent to analyzing particle trajectories in a simulation or experiment on sedimentation, as there the distribution of particles across the side walls presumably reaches some steady state whose properties are presently unknown. Figure 5 already showed the path of a typical particle falling in a blob of width $10a$; Fig. 10 shows the path of the same particle falling through a cell with width $20a$. The initial volume fraction in both simulations is identical $\phi_0 = 0.1$. In both sets of simulations it is seen that the particle wiggles around the cell, as it does in the Nicolai *et al.* experiments.^{13,14} The scale of the wiggling in the two simulation figures is clearly set by the cell width; in both sets of simulations when viewed from the top the scale of the wiggling is about $D/2$. Similarly, in the Nicolai *et al.* experiments (e.g., Fig. 1 of Ref. 13), the scale of the wiggling is about $40a$ whereas the cell half-width is about $50a$. In addition, the time it takes for the particle to collide with the wall

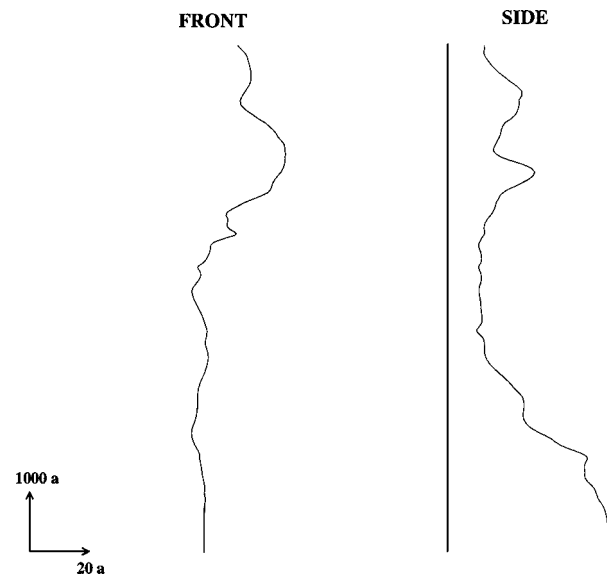


FIG. 10. Top and side view of a particle path in the blob disintegration simulation shown above. The scales in the \hat{y} and \hat{x} direction are the same ($20a$), whereas the scale in the falling \hat{z} direction is compressed. Note that the fluctuations in the trajectory in the plane perpendicular to the side walls is of the order of the fluctuations in the trajectory between the walls.

is about double in the $D = 20a$ cell than the $D = 10a$ cell. Figure 11 compares the \hat{x} and \hat{y} components of the velocity for the two cells. It is seen that, although initially the velocity fluctuations for the particle in the $D = 20a$ cell are larger than those in the $D = 10a$ cell, eventually they both settle down to velocity fluctuations in the range of about $0.1U_s$.

We do not want to interpret these results too literally, as there are serious differences between our simulation and sedimentation, as noted above. However, this set of simulations clearly suggests another possible resolution of the contradiction between our arguments about the importance of wall effects and the Nicolai–Guazzelli experiments' i.e., that it is possible that long time measurements of single particle diffusivities do not sample the maximal velocity fluctuations in the cell.

This latter interpretation also provides a consistent rationalization for the more recent measurements of Peysson and Guazzelli,³² who verified that in the $D = 40\text{ mm}$ cell the size of the fluctuations and the correlation time are independent of the width of the cell, when it is varied from $4 \rightarrow 10\text{ cm}$, with the depth fixed at 4 cm . They also demonstrated that the size of the fluctuations is independent of the position along the width of the cell, except for layer of width $\approx 0.2W$ near the side walls (bounding the width). These measurements are consistent with our arguments: The size of the fluctuations will be controlled by the *shortest* dimension of the cell. Therefore varying the width (when $W \gg D$) should have little effect on the size of the fluctuations. Correspondingly, since the measurements represent averages across the cell depth, there should not be any variation of the fluctuations across the width of the cell until the particles sampled are of order $D/2 = 2\text{ cm}$ from the side walls (bounding the width). In Fig. 2 of Ref. 32 the fluctuations vary within a layer $0.2W$

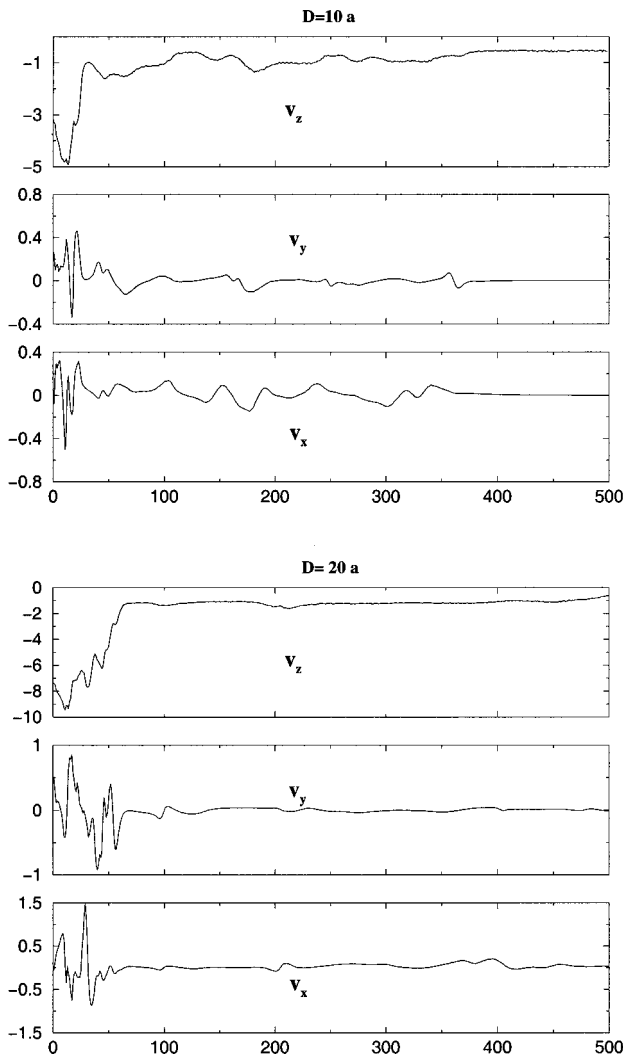


FIG. 11. Time dependence of the components of the particle velocities depicted in Figs. 5 (upper figure) and 10 (lower figure). The size of the velocity fluctuations is initially larger in the $D=20a$ cell (lower figure) but at long times the size of fluctuations for the two cells is essentially identical.

= 2 cm from the side wall, as expected from this simple argument.

C. Summary of this section

To summarize the results of this section, we have presented theory, numerical simulations, and scaling arguments illustrating how confinement by rigid walls can produce non-trivial scaling laws for the correlation length and velocity fluctuations of a sedimenting flow at low volume fractions. Based on these ideas, we have argued that current experiments do not definitively exclude the divergence of the velocity fluctuations with system size, although they do imply the divergence is weaker than the Caffisch–Luke law suggests.

Our arguments suggest at least two different regimes for $\Delta U(\phi)$, depicted pictorially in Fig. 3. These regimes imply that the velocity fluctuations should have the qualitative behavior sketched in Fig. 12. For $\phi < N_{\text{blob}}\phi_* = \phi_{\text{crit}}$, the particle interactions are weak enough that the $\Delta U \sim \sqrt{\phi}$ law is

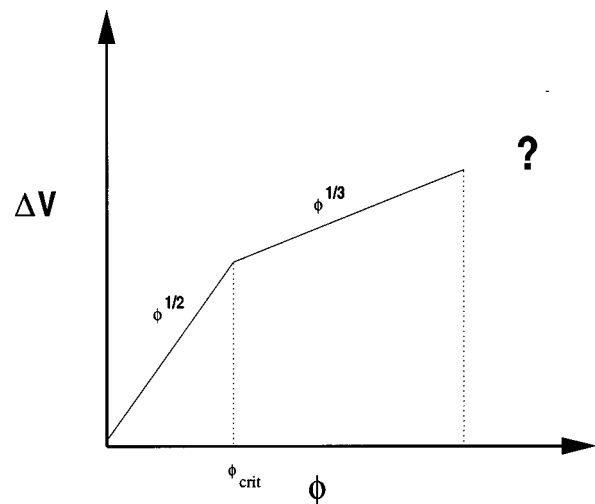


FIG. 12. Sketch of the different scaling regimes proposed, on a double logarithmic plot. For $\phi < \phi_{\text{crit}}$ the velocity fluctuations should scale like $\sqrt{\phi}$. For $\phi_{\text{crit}} < \phi \Delta U \sim \phi^{1/3}$.

obeyed. Above ϕ_{crit} the $\phi^{1/3}$ law is obeyed. The critical volume fraction ϕ_* has only a single particle per interaction volume. The volume fraction ϕ_{crit} has N_{blob} particles per interaction volume, and controls the crossover in the experiments. Both of these numbers depend strongly on the shape of the container. To our knowledge, the transition between these two regimes in a single cell has not yet been observed. We propose that the smallest cells used in Ref. 15 lie in the first $\sqrt{\phi}$ regime, whereas the larger cells lie in the second regime. Besides varying ϕ at fixed cell size, this general picture could be directly tested by studying the scaling laws for the velocity fluctuations as a function of distance from the wall of the cell: close to the wall, the $\sqrt{\phi}$ law should hold and a transition should appear when the sampling volume is far enough from the walls. Finally, we remark that since all of our arguments are based on the long ranged part of the particle greens function, their applicability at higher volume fractions is unclear.

D. Inertial screening

We now turn to a brief description of another mechanism for screening the velocity fluctuations. Although we do not believe that this mechanism applies to the present experiments, it illustrates another example of a screening argument which relies on a cutoff of the slow decay of the Oseen tensor, instead of a structural transition in the particles distribution. We also consider this mechanism as a plausible possibility for the infinite system size limit, where wall effects are not important.

Consider a sedimenting mixture in a box large enough so that the wall effects discussed above do not apply. The Caffisch–Luke–Hinch argument suggests that the velocity fluctuation diverges with system size, and hence that the particle diffusivity \mathcal{D} diverges with system size. The idea of inertial screening is that, eventually, the particle diffusion constant \mathcal{D} will become of order of the momentum diffusion constant

$$D \sim \nu. \tag{17}$$

At this point, particles will diffuse faster than the momentum they are releasing into the fluid, and momentum transport away from particles is no longer effective, so that the $\bar{u} \sim r^{-1}$ law will not apply. This provides a cutoff for the size of the velocity fluctuations.

Scaling laws for the dependence of the correlation length and velocity fluctuations on both the particle Reynolds number Re_p and ϕ can then be constructed by balancing $D \sim \nu$ and using the Caflisch–Luke formula (5) as above. Details of how this works depend on how one estimates the diffusion constant \mathcal{D} . For illustrative purposes, we list the results of such an estimate here. (Although we emphasize that, in the absence of a detailed theory for the diffusivity, these formulae are speculative.) In general, the diffusivity is $D \sim \Delta U^2 \tau$, where τ is the correlation time. If the correlation time is set by the time for a particle to move across a blob, then $\tau \sim l/\Delta U$ and then $D \sim \Delta U l$. Setting $D \sim \nu$ and combining with the Caflisch–Luke argument as above gives the scaling laws

$$l = a(Re_p)^{-2/3} \phi^{-1/3}, \tag{18}$$

$$\frac{\Delta U}{U_s} = Re_p^{1/3} \phi^{1/3}, \tag{19}$$

$$N_{\text{blob}} \sim Re_p^{-2}. \tag{20}$$

Hinch⁹ previously gave another argument for these scaling laws by proposing there might be a finite Reynolds number instability of a falling blob. The argument leading to Eq. (17) gives a more precise criterion for when inertia is necessarily important during sedimentation. The correct scaling laws for l and ΔU would follow from this approach by determining \mathcal{D} self consistently.

Another approach toward inertial screening has previously been described by Koch,³³ for a sediment falling at moderate Reynolds numbers $Re_p \approx 1$. His arguments utilize the single particle Oseenlet to cut off the divergence. It turns out that this is not quite enough: in the Oseen solution the velocity decays like r^{-2} everywhere except a small wake, which causes a logarithmic divergence in ΔU . Koch argues that this divergence is cancelled by the relative motion of two particles out of each others wake by a lift force. The scaling laws derived by Koch differ from those given above. A difference between his treatment and the argument given here is that the present is designed to work in the limit of $Re_p \rightarrow 0$, whereas his argument works at $Re_p \sim 1$.

We are confident that inertia is not playing a role in either of the two sets of experiments discussed herein; the reason for this assertion is simply that all previous experiments are either (a) in a regime where simple estimates indicate that wall effects are important, or (b) very close to the regime where wall dominated effects are important. However, in the limit of infinite system size, inertially dominated screening is a plausible theoretical possibility.

IV. COUPLING TO MEAN VELOCITY

We now return to the question of the dependence of the mean sedimenting velocity U_{sediment} on ϕ . The formula of Burgers and Batchelor^{3,4} ignores the velocity fluctuations and only counts two particle interactions; it is thus natural to ask whether corrections arise from the fluctuations. Recall that a blob of $N_{\text{blob}} \pm \sqrt{N_{\text{blob}}}$ particles moves downward at velocity $U_s \mp \Delta U$. Since more particles fluctuate downward than upward, blobs contribute a net downward volume flux of particles $c \sqrt{N_{\text{blob}}} \Delta U v_p / l^3$, where c is a constant of order unity. Hence, there is a correction to U_{sediment} of $\sqrt{N_{\text{blob}}} \Delta U v_p / l^3 / \phi = c \Delta U / \sqrt{N_{\text{blob}}}$, so

$$U_{\text{sediment}} = U_s \left(1 - 6.55 \phi + \frac{c}{\sqrt{N_{\text{blob}}}} \frac{\Delta U}{U_s} + \dots \right). \tag{21}$$

The central consequence of this formula is that, depending on the screening mechanism, fluctuation induced transport could dominate the backflow correction to the sedimentation.

We now discuss the implications of this result for the Segré *et al.* experiments. The confinement induced screening mechanism implies that the correction to the sedimenting velocity is of order $(2a/D)^{2/3} \phi^{1/3}$. There are two interesting features of this result: first, it indicates that in the limit $\phi \rightarrow 0$ the fluctuation contribution to the sedimenting velocity dominates; second, it demonstrates that the sedimenting velocity depends (albeit weakly) on the shape of the container. Previous studies¹⁹ addressing whether the sedimentation velocity depends on the container shape have examined only the backflow contribution.

The crossover between the backflow contribution and the fluctuation contribution to U_{sediment} occurs when $\phi \sim 0.06(2a/D) \sim 10^{-3}$ in Segré *et al.* This volume fraction is so small as to be irrelevant for most experiments. However, experiments^{1,7} typically measure a coefficient of the $O(\phi)$ term which is systematically smaller in magnitude than 6.55. Writing $U_{\text{sediment}} = U_s (1 - (6.55 - c(2a/D)^{2/3} \phi^{-2/3}) \phi)$ shows that a linear fit to the data with $2a/D = 10^{-2}$ and $\phi = 10^{-2}$ will give a coefficient of approximately $6.55 - 10^{-4/3} \times 10^{+4/3} = 5.55$, which is in the range of what is normally observed. It should also be remarked that this argument provides a rationalization for why different experiments tend to observe different values for the coefficient of the $O(\phi)$ terms: The contribution of the velocity fluctuations to the mean velocity implies that the different formulae could apply to different cell geometries. The other argument that is usually invoked for explaining the systematically smaller magnitude of the $O(\phi)$ term than Batchelor’s argument suggests is that a real system has some degree of polydispersity.

V. DISCUSSION AND CONCLUSIONS

The most basic question in sedimentation is to link the “microscopic” description of many particles interacting hydrodynamically in a Stokes flow with a macroscopic description, as envisioned by Kynch:³⁴

$$\partial_t \phi + \partial_z (U(\phi) \phi) = \nabla \cdot (D(\phi) \nabla \phi), \tag{22}$$

where here ϕ is the local volume fraction, $U(\phi)$ is the local advection velocity, and $D(\phi)$ is the local diffusivity. This type of description is enormously successful in describing the local properties of systems (like non-Newtonian fluids) where thermal fluctuations are important, so the diffusivity is dominated by the Stokes–Einstein relation. The fundamental question is to determine whether this type of effective hydrodynamic description still applies in the limit where thermal fluctuations become irrelevant.

Classical theories of sedimentation^{2–4} aimed to predict $U(\phi)$. The original theoretical difficulty was that simple estimates of $U(\phi)$ led to divergent answers. This problem is due to a real physical effect: The velocity a blob of sediment at constant volume fraction surrounded by an infinite fluid increases with increasing blob size according to $U \sim u_s \phi R^2$. Batchelor⁴ realized that in an actual experiment, container boundaries force the backflow to flow through sediment, which imposes a constraint which cuts off the divergence. This constraint leads to a convergent answer for $U(\phi)$, which Batchelor finds to be essentially independent of the properties of the container.

The screening of velocity fluctuations is the analogue of this same problem for determining the effective diffusivity $D(\phi)$. The principal goal of this paper was to explore the effects of container walls on controlling the size of the velocity fluctuations. Previous theories of sedimentation have assumed that the system is infinite and homogeneous in the direction transverse to the settling, and therefore neglected the dynamical effect of container walls. The principle wall effect is due to the well known fact that there is a transition in the flow field around a particle at a distance from the particle of order the particle-wall distance. This transition implies that, when a particle moves around a cell, the number of particles with which it is effectively interacting changes. Through scaling arguments and simulations we have argued that side walls lead to a number of important consequences: (1) There are at least two different regimes of sedimentation, i.e., the weakly interacting regime and the strongly interacting regime. The transition between these two regimes occurs at a critical volume fraction (for fixed cell geometry) or at a critical cell depth (at fixed volume fraction). (2) The size of the velocity fluctuations acquires a dependence on the distance from the wall. This could result in a nonuniform particle distribution across the cell, and also implies a variation in the effective properties of the sediment across the cell. (3) Side walls even affect two particle interactions, by breaking the usual symmetry that implies that in an infinite system two sedimenting particles maintain a constant distance from each other. On the basis of our analysis, we have argued that current experiments have not definitively excluded the dependence of the velocity fluctuations on the size of the cell, although they have demonstrated that if the divergence exists it must be weaker than the Caffisch–Luke prediction.

The sedimentation experiments that we are aware of typically visualize the sediment by projecting the particle motion onto a plane perpendicular to the shortest dimension of the cell. The smallest dimension of experimental cells is typically of order 50 particle diameters, which is small

enough that it is still possible to transmit light through the system. From the arguments presented herein, it appears to us that at these dimensions the wall effects will be crucial for determining critical features of the flow. Examples of this go beyond that of monodisperse sedimentation of spheres: for example, Batchelor and van Rensberg's study³⁵ of clumping instabilities in bidisperse suspension uses a cell width of 3–5 mm, with particles of size about 0.3 mm. From their photographs the initial scales of the instabilities they observe are a few millimeters across. Similarly, Herzhaft *et al.*'s study³⁶ of clumping instabilities in fiber suspensions take place in cells with $D/a \approx 40$ as the observed clump sizes are in the range of $D/2$. It is unclear to us whether a theoretical treatment based on an infinite homogeneous system is appropriate for analyzing either of these experiments.

One of the major concerns in trying to derive an effective theory for the sediment is that it is crucial that there be a scale separation between the region where bulk equations [like Eq. (22)] apply and the region where an effective boundary conditions apply. In non-Newtonian fluids this scale separation is ensured by thermal fluctuations: the Brownian motion of an object very far from a wall ensures that the effect of the wall on the motion is incoherent. In the present problem, the interactions of single particles both with each other and with the boundaries are long ranged so that whether a natural scale separation exists is unclear. This issue is perhaps a purely theoretical concern; e.g., Acrivos and collaborators (see, e.g., Ref. 37) have successfully applied phenomenological slip boundary conditions to different types of sedimenting flows, with excellent agreement between theory and experiments.

Our interest in these general questions was initiated by recent experiments by Segré *et al.*¹⁵ and Nicolai and Guazzelli.¹⁴ A simple scaling theory for the first mechanism—based on confinement in cells of high aspect ratio—was introduced and shown to be in reasonable agreement with the recent experiments of Segré *et al.*;¹⁵ the ideas presented herein appear to be in contradiction to the conclusions of Nicolai and Guazzelli,¹⁴ and several possible resolutions are proposed. Several of our predictions could be tested experimentally.

Finally, our study gives a simple scaling argument which suggests that in general there is a coupling between the fluctuations and the mean settling velocity. This fluctuation induced correction to the mean velocity has the opposite sign as the backflow contribution, and could provide another explanation for why experiments⁷ systematically observe a lower coefficient of the $O(\phi)$ correction than that predicted by Burgers and Batchelor.^{3,4} Coupled with the various screening mechanisms proposed herein, it also suggests that the dependence on the fluctuations on cell geometry or particle Reynolds number should be reflected in the mean settling velocity.

ACKNOWLEDGMENTS

I am grateful to Howard Stone for many important discussions, to John Hinch for stimulating criticisms, to Phil Segré for discussions about his experiments, and to John

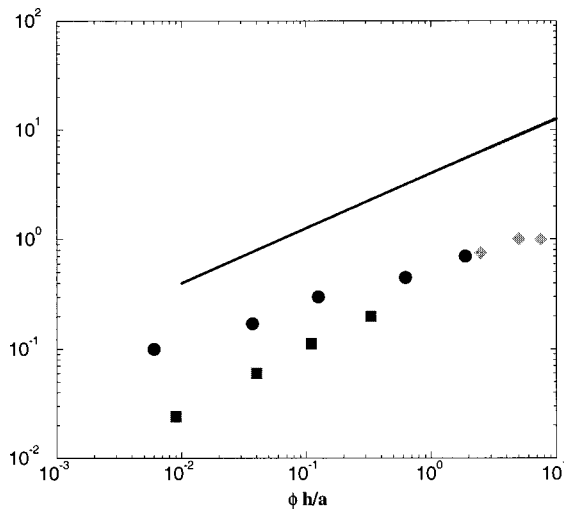


FIG. 13. Comparison of the theoretical upper bound (thick solid line), given by Eq. (A7) to existing experimental data. The circles are the data from Fig. 3 of Ref. 15, for large cells. The squares are the data from the 3 mm×0.3 mm cells of Ref. 15. The diamonds are the smallest volume fraction data from Ref. 13. The experiments are systematically below this upper bound.

Crocker, Daniel Fisher, Don Koch, and Marteen Rutgers for helpful comments. Acknowledgment is made to the A. P. Sloan Foundation, the National Science Foundation, and to the Donors of The Petroleum Research Fund, administered by the American Chemical Society, for partial support of this research.

APPENDIX A: UPPER BOUNDS FOR VELOCITY FLUCTUATIONS

The goal of this appendix is to estimate the upper bound for the size of the velocity fluctuations in the vicinity of a single wall, assuming that the particle configuration is random. Our aim in putting forth this calculation is not mathematical rigor, but instead to provide a ball park estimate to assess when walls are important in a given experimental configuration. The result of the calculation is shown in Fig. 13.

We consider an experiment which samples the fluctuations a distance h from a rigid wall, where the sedimenting direction is parallel to the wall, and determine an estimate for the upper bound on ΔU as a function of h . The solution for the problem of a point force near a plane rigid boundary was first written down by Lorenz,²⁴ and later by Blake.²² This problem differs slightly from a particle translating near a rigid wall; a spherical particle differs from a point force by corrections of order $(a/r)^2$, where a is the particle radius, and r the distance from the particle. We will see in the following that these terms give only higher order corrections to the upper bound, and so can be neglected at leading order.

Consider a coordinate system (x_1, x_2, x_3) with a plane wall located at $x_1=0$, and a particle moving in the x_3 direction located at $\mathbf{r}_0=(w_1, w_2, w_3)$. We seek the solution to

$$\mu \nabla^2 \mathbf{u} = \nabla p + F \hat{x}_3 \delta(\mathbf{r} - \mathbf{r}_0), \tag{A1}$$

$$\nabla \cdot \mathbf{u} = 0, \tag{A2}$$

with μ the fluid viscosity, $F = 6\pi\mu U_s a$ is the force in the \hat{x}_3 direction, and the fluid velocity is required to vanish at the wall. Without the boundary condition on the wall, the solution to this problem is

$$\mathbf{u} = \frac{F \hat{z}}{8\pi\mu} \cdot \left(\frac{\delta_{i,j}}{r} + \frac{r_j r_k}{r^3} \right), \tag{A3}$$

where $\delta_{i,j}$ is the identity matrix, $r = |\mathbf{r} - \mathbf{r}_0|$, and r_j are the components of $\mathbf{r} - \mathbf{r}_0$. The boundary condition of the wall is accounted for using image singularities. Blake's solution is

$$\mathbf{u} = \frac{F \hat{z}}{8\pi\mu} \cdot \left(\frac{\delta_{i,j}}{r} + \frac{r_j r_k}{r^3} - \frac{I}{R} - \frac{R_j R_k}{R^3} + \left[2r_1 (\delta_{k,\alpha} \delta_{\alpha,l} - \delta_{k,l} \delta_{1,l}) \frac{\partial}{\partial R_l} \left(\frac{r_1 R_j}{R^3} - \frac{\delta_{j,1}}{R} + \frac{R_j R_1}{R^3} \right) \right] \right), \tag{A4}$$

where R_i are the components of $\mathbf{R} = (x_1, x_2, x_3) + \mathbf{r}_0$, the position of the image. The part of the formula contained in square brackets represents higher order dipolar corrections. These are necessary because the difference between the two image Stokeslets does not cancel out perfectly on the planar boundary. Notice that this formula has the feature that, far from the particle, the image Stokeslet cancels out the leading order r^{-1} decay of the force, and hence the decay is like r^{-2} .

As remarked upon above, this solution represents the fluid velocity produced by a point force, which is not quite the same as the velocity field produced by a sphere. There are higher order corrections $O(r^{-2})$ to the point force solution arising from the boundary condition on the sphere. Hence, although this solution has the correct qualitative properties of the flow around a sphere falling near a wall, the correct formula will contain further dipolar corrections, so that the terms in the square brackets in Eq. (A4) will be modified. However, these terms only contribute an $O(a/h)$ correction to the upper bound.

The velocity fluctuations sampled a distance h from the wall follows from

$$\Delta U^2 = \frac{3\phi}{8\pi a^3} \int d^3 r' \mathbf{u}(\tilde{\mathbf{r}} - \mathbf{r}')^2, \tag{A5}$$

where $\tilde{\mathbf{r}} = (h, 0, 0)$, and the integral is over all space. By rescaling $\mathbf{r}' \rightarrow h\mathbf{w}$, and using $F = 6\pi\mu U_s a$, this integral becomes

$$\Delta U^2 = U_s^2 \frac{27\phi h}{64 a} I,$$

where I is given by the integral

$$I = \int d^3 w (8\pi F \mathbf{u}(\tilde{\mathbf{w}} - \mathbf{w}))^2, \tag{A6}$$

where $\tilde{\mathbf{w}} = (1, 0, 0)$ and again the integral is over all space. Hence, determining the upper bound requires determining the value of the single integral I . This integral was evaluated using the numerical integration procedures in Mathematica to be $I = 37.3$. This implies the upper bound

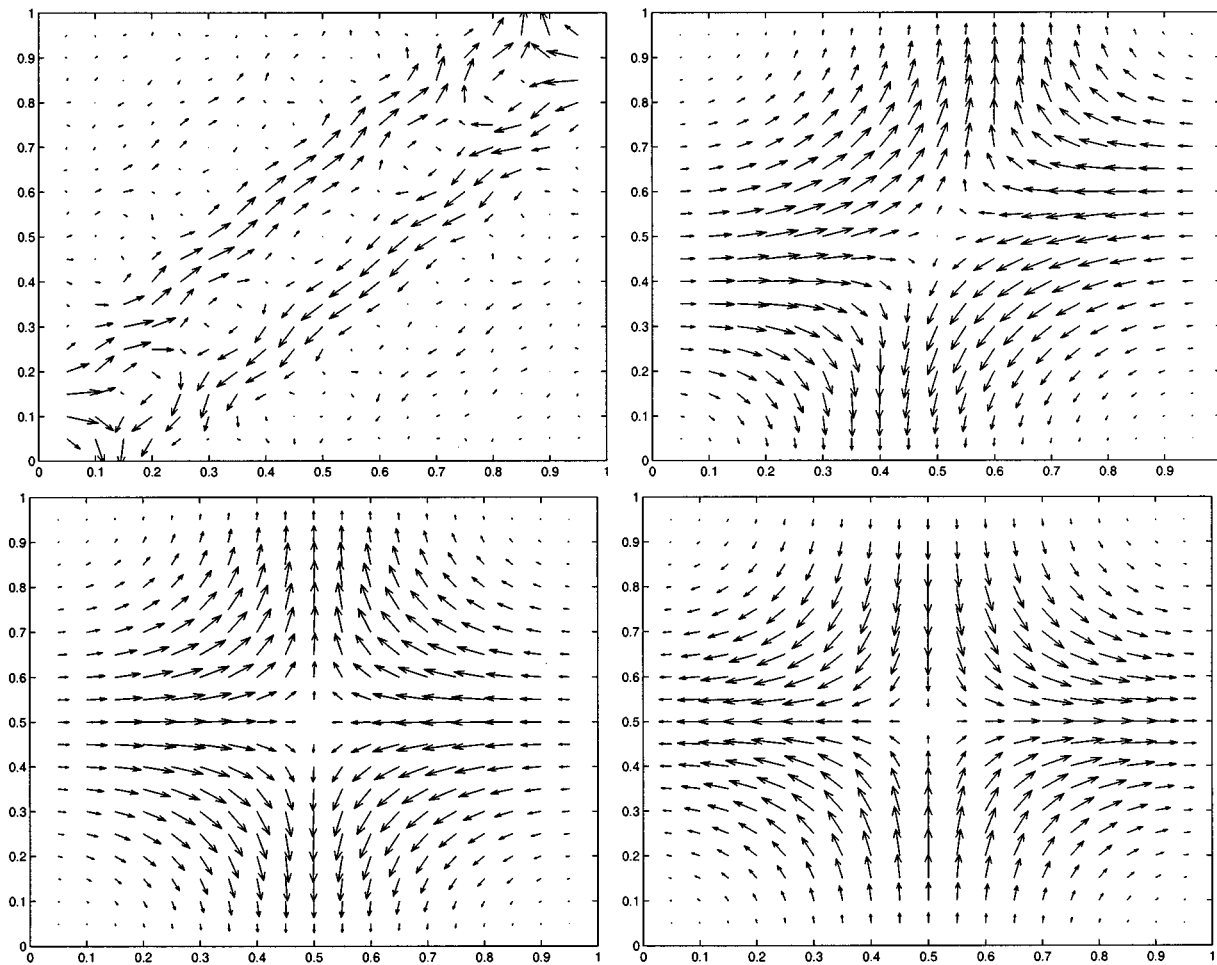


FIG. 14. Phase plane of the of the particle trajectories in the $x_1 - x_2$ plane of two particles with locations $x = x_1$ and $x = x_2$. The particles are falling between two solid plates located at $x = 0$ and $x = 1$. The upper left picture denotes $\rho = 0.1$, the upper right denotes $\rho = 0.5$, the bottom left $\rho = 1$ and the bottom right $\rho = 5$.

$$\frac{\Delta U}{U_s} \approx 4\sqrt{\phi} \sqrt{\frac{h}{a}}. \quad (\text{A7})$$

Figure 13 compares this upper bound to existing experimental data. In the comparison, we take the value of h to be the half the shortest dimension of the container.

The most severe approximation of this calculation is that it only accounts for a *single* wall, whereas multiple walls affect the experiments. The influence of a second wall can be surprisingly strong. For a particle falling between two parallel plates of spacing D an exact solution was found by Liron and Mochon.²⁶ In comparing the solution for the two plates to the solution for a single plate, they noted that there are quantitative discrepancies in the single wall calculation unless the particle is closer than a distance $D/8$ to one of the walls.

APPENDIX B: TWO POINT FORCES BETWEEN TWO WALLS

Section III demonstrates through direct numerical simulation that side walls can have a dramatic effect on a sedimenting flow. Here, we examine the much simpler question of how sidewalls can influence the trajectories of *two* par-

ticles (represented as point forces) falling relative to each other, and demonstrate that even in this case the side walls have an important effect.

A basic fact about sedimentation is that two particles falling in infinite space do not move relative to each other. The reason for this follows directly from symmetry: The influence of the first particle on the second is exactly the same as the influence of the second particle on the first. In formulas, if we represent each particle by a point force, the fluid velocity is $\mathbf{u} = \mathbf{S}_p(\mathbf{r} - \mathbf{r}')$, where \mathbf{S}_p is the single particle Stokeslet, defined in Sec. III. The velocity of the particles can then be expressed as

$$\dot{\mathbf{x}}_1 = U_s \hat{\mathbf{z}} + \mathbf{S}_p(\mathbf{x}_1 - \mathbf{x}_2), \quad (\text{B1})$$

$$\dot{\mathbf{x}}_2 = U_s \hat{\mathbf{z}} + \mathbf{S}_p(\mathbf{x}_2 - \mathbf{x}_1). \quad (\text{B2})$$

Subtracting Eq. (B1) from (B2) implies that $\mathbf{x}_1 - \mathbf{x}_2$ is a constant.

The presence of side walls breaks the symmetry in the direction perpendicular to the walls. Here we address how this symmetry breaking affects the relative motion between two particles. To do this, we need a representation of the Stokeslet \mathbf{S} for a particle falling between two walls. For this purpose it is efficient to use the exact formulas written down

by Liron and Mochon (Ref. 26). (Comparing the results from the exact formula to the model formula used in the many particle simulations above, it turns out that the two formulas give qualitatively similar answers. This provides an important check on the validity of our model formula.)⁵ If the walls are located at $x=0$ and $x=L$, and the particles fall along \hat{z} , the solution demonstrates that both $\mathbf{S}(\mathbf{x}_1, \mathbf{x}_2) \cdot \hat{z}$ and $\mathbf{S}(\mathbf{x}_1, \mathbf{x}_2) \cdot \hat{y}$ are symmetric with respect to interchange of \mathbf{x}_1 and \mathbf{x}_2 . This implies that both the relative \hat{y} and \hat{z} separa-

tion of the two particles is *fixed* during the particle motion.

However, the Liron–Mochon solution shows that this symmetry is broken for $\mathbf{S} \cdot \hat{x}$, so that there will be relative motion along the \hat{x} direction. Here, we use their solution to characterize the orbits of the two particles relative to each other along the \hat{x} direction. Their solution²⁶ for the fluid velocity at \mathbf{x}_2 given a particle at \mathbf{x}_1 is

$$\begin{aligned} \mathbf{S}(\mathbf{x}_1, \mathbf{x}_2) \cdot \hat{x} = & -\frac{1}{4\pi} \frac{z_2 - z_1}{\rho} \operatorname{Im} \sum_{m=1}^{\infty} \frac{z_m H_1^{(1)}(\rho z_m)}{\sqrt{1+z_m^2} - 1} (x_1 x_2 z_m (\sinh(z_m(x_2 - x_1)) - z_m \cosh(z_m(x_1 + x_2))) \\ & + \sqrt{1+z_m^2} \sinh(z_m(x_1 + x_2))) + z_m(x_2 \cosh(x_2 z_m) \sinh(x_1 z_m) - x_1 \sinh(x_2 z_m) \cosh(x_1 z_m)) \\ & + \sinh(x_1 z_m) \sinh(x_2 z_m) ((x_1 - x_2) \sqrt{1+z_m^2} - (x_1 + x_2 - L))). \end{aligned} \tag{B3}$$

Here $\rho = \sqrt{(y_2 - y_1)^2 + (z_2 - z_1)^2}$ and z_m are the complex roots of $\sinh(z)^2 = z^2$. We have expressed the particle positions x_1 and x_2 in units of the plate spacing l_0 . The relative particle motion of the particles is then governed by

$$\dot{x}_1 = \mathbf{S}(\mathbf{x}_2, \mathbf{x}_1) \cdot \hat{x}, \tag{B4}$$

$$\dot{x}_2 = \mathbf{S}(\mathbf{x}_1, \mathbf{x}_2) \cdot \hat{x}. \tag{B5}$$

The nature of the dynamics depends on the relative particle spacing parallel to the plates, ρ . Figure 14(a)–(d) shows the phase planes of the trajectories in the $x_1 - x_2$ plane for $\rho = 0.1, 0.5, 1$, and $\rho = 5$. In each case, the phase planes show that the particles tend to move relative to each other $x_1 - x_2$ plane. It is important to note that the time scale of the motion depends on both ρ and $(z_2 - z_1)$, and is logically unrelated to the characteristic time scale for falling aU_s^{-1} . The time scale scales roughly like $(z_2 - z_1)/\rho^2$ when $\rho < 1$, so that when $\rho \sim 1$ it is of order $aU_s^{-1}(D/a)$. When $\rho \gg 1$ the time scale increases exponentially with ρ . Physically, when one particle is pushed to a wall the other can fall unimpeded.

An important feature of these phase planes is the change in the structure as $\rho \rightarrow 0$. This corresponds to taking the infinite system limit, and making the distance between the walls much larger than the distance between the two particles. We know that in this limit, the distance between the two particles must become fixed. This implies that every point in the $x_1 - x_2$ plane must become a fixed point when $\rho \rightarrow 0$. The beginnings of this transition are apparent in Fig. 14.

⁴G. K. Batchelor, ‘‘Sedimentation in a dilute dispersion of spheres,’’ *J. Fluid Mech.* **52**, 245 (1972).

⁵G. K. Batchelor, *An Introduction to Fluid Dynamics* (Cambridge University Press, Cambridge, 1967).

⁶E. J. Hinch, ‘‘An averaged-equation approach to particle interactions in a fluid suspension,’’ *J. Fluid Mech.* **83**, 695 (1977).

⁷R. H. Davis and A. Acrivos, ‘‘Sedimentation of noncolloidal particles at low Reynolds numbers,’’ *Annu. Rev. Fluid Mech.* **17**, 91 (1985).

⁸R. E. Caflisch and J. H. C. Luke, ‘‘Variance in the sedimentation speed of a suspension,’’ *Phys. Fluids* **28**, 259 (1985).

⁹E. J. Hinch, in *Disorder in Mixing*, edited by E. Guyon *et al.* (Kluwer Academic, Dordrecht, 1988), p. 153.

¹⁰A. J. C. Ladd, ‘‘Hydrodynamic screening in sedimenting suspensions of non-Brownian spheres,’’ *Phys. Rev. Lett.* **76**, 1392 (1996).

¹¹A. J. C. Ladd, ‘‘Sedimentation of homogeneous suspensions of non-Brownian spheres,’’ *Phys. Fluids* **9**, 491 (1997).

¹²J. M. Ham and G. M. Homsy, ‘‘Hindered settling and hydrodynamic dispersion in quiescent sedimenting suspensions,’’ *Int. J. Multiphase Flow* **14**, 533 (1988).

¹³H. Nicolai and E. Guazzelli, ‘‘Effect of the vessel size on the hydrodynamic diffusion of sedimenting spheres,’’ *Phys. Fluids* **7**, 3 (1995).

¹⁴H. Nicolai, B. Herzhaft, E. J. Hinch, L. Oger, and E. Guazzelli, ‘‘Particle velocity fluctuations and hydrodynamic self-diffusion of sedimenting non-Brownian spheres,’’ *Phys. Fluids* **7**, 12 (1995).

¹⁵P. N. Segre, E. Herbolzheimer, and P. M. Chaikin, ‘‘Long ranged correlations in sedimentation,’’ *Phys. Rev. Lett.* **79**, 2574 (1997).

¹⁶D. L. Koch and E. S. G. Shaqfeh, ‘‘Screening in sedimenting suspensions,’’ *J. Fluid Mech.* **224**, 275 (1991).

¹⁷J. Happel and H. Brenner, *Low Reynolds Number Hydrodynamics, with Special Applications to Particulate Media* (Prentice Hall, Englewood Cliffs, NJ, 1965).

¹⁸D. L. Koch, ‘‘Hydrodynamic diffusion in a suspension of sedimenting point particles with periodic boundary conditions,’’ *Phys. Fluids* **6**, 2894 (1994).

¹⁹C. W. J. Beenakker and P. Mazur, ‘‘Is sedimentation container shape dependent?’’ *Phys. Fluids* **28**, 3203 (1985).

²⁰E. M. Tory, M. T. Kamel, and C. F. Chan Man Fong, ‘‘Sedimentation is container-size dependent,’’ *Powder Technol.* **73**, 219 (1992).

²¹P. G. Saffman, ‘‘On the settling speed of free and fixed suspensions,’’ *Stud. Appl. Math.* **52**, 115 (1973).

²²J. R. Blake, ‘‘A note on the image system for a stokeslet in a no slip boundary,’’ *Proc. Cambridge Philos. Soc.* **70**, 303 (1971).

²³J. Blake, ‘‘A model for the micro-structure in ciliated organisms,’’ *J. Fluid Mech.* **52**, 1 (1972).

²⁴H. A. Lorenz, ‘‘Ein allgemeiner satz, die bewegung einer reibenden flussigkeit betreffend, nebst einigen anwendungen desselben,’’ *Abhand. Theor. Phys. (Leipzig)* **1**, 23 (1907).

¹R. H. Davis, in *Sedimentation of Small Particles in a Viscous Fluid*, edited by E. M. Tory (Computational Mechanics Publications, Southampton, 1996).

²M. Smoluchowski, ‘‘On the practical applicability of Stokes’ law,’’ *Proceedings of the 5th International Congress on Mathematics* **2**, 192 (1912).

³J. M. Burgers, ‘‘On the influence of the concentration of a suspension upon the sedimentation velocity,’’ *Proc. Kon. Nederl. Akad. Wet.* **44**, 1045 (1942).

- ²⁵C. Pozrikidis, *Boundary Integral and Singularity Methods for Linearized Viscous Flow* (Cambridge University Press, Cambridge, 1992).
- ²⁶N. Liron and S. Mochon, "Stokes flow for a stokeslet between two parallel flat plates," *J. Eng. Math.* **10**, 287 (1976).
- ²⁷N. J. De Mestre, "Low Reynolds number fall of slender cylinders near boundaries," *J. Fluid Mech.* **58**, 641 (1973).
- ²⁸J. Blake, "On the generation of viscous toroidal eddies in a cylinder," *J. Fluid Mech.* **95**, 109 (1979).
- ²⁹N. Liron, "Stokes flow due to a Stokeslet in a pipe," *J. Fluid Mech.* **86**, 727 (1978).
- ³⁰L. J. Durlofsky and J. F. Brady, "Dynamics simulation of bounded suspensions of hydrodynamically interacting particles," *J. Fluid Mech.* **200**, 39 (1989).
- ³¹J. M. Nitsche and G. K. Batchelor, "Break-up of a falling drop containing dispersed particles," *J. Fluid Mech.* **240**, 161 (1997).
- ³²Y. Peysson and E. Guazzelli, "An experimental investigation of the intrinsic convection in a sedimenting suspension," *Phys. Fluids* **10**, 44 (1997).
- ³³D. L. Koch, "Hydrodynamic diffusion in dilute sedimenting suspensions at moderate Reynolds numbers," *Phys. Fluids* **5**, 1141 (1993).
- ³⁴Kynch, "A theory of sedimentation," *Trans. Faraday Soc.* **48**, 166 (1951).
- ³⁵G. K. Batchelor and R. W. Janse Van Rensburg, "Structure formation in bidisperse sedimentation," *J. Fluid Mech.* **166**, 379 (1986).
- ³⁶B. Herzhaft, E. Guazzelli, M. Mackaplow, and E. S. G. Shaqfeh, "Experimental investigation of the sedimentation of a dilute fiber suspension," *Phys. Rev. Lett.* **77**, 290 (1996).
- ³⁷B. Kapoor and A. Acrivos, "Sedimentation and sediment flow in settling tanks with inclined walls," *J. Fluid Mech.* **290**, 39 (1995).